Spin Exchange Relaxation Free (SERF) Magnetometers

Igor Mykhaylovich Savukov

Abstract A little more than a decade ago spin-exchange relaxation free (SERF) magnetometers set a new record of magnetic field sensitivity surpassing cryogenic SQUIDs. Since then a lot of progress has been made in design, commercialization, and development of novel applications of the SERF magnetometers. In addition, the operation of the SERF magnetometer was extended beyond the SERF regime resulting in the discovery of ultra-high sensitivity high frequency and scalar magnetometers. This chapter will cover some basic principles of SERF and high-density SERF-like magnetometers in the regimes when spin-exchange collisions affect the line-width of the magnetometers. Various topics will be covered: the SERF operation, the role of spin-exchange collisions, fundamental and technical noises in SERF and other high-density magnetometers, light shifts, optical pumping. The formalism of density matrix equations will be briefly described with some illustrations. At some conditions, Bloch equations can also provide adequate treatment of spin dynamics, so this topic is also briefly covered. Some applications, such as magnetoencephalography and magnetic resonance imaging (MRI), of SERF, high-frequency, and scalar magnetometers will be discussed. The number of applications will grow in the future, especially when high-sensitivity SERF magnetometers become commercially available and their operation becomes simple and user-friendly. Finally, it is anticipated that in the near future many applications developed with SQUIDs will be gradually replaced with those based on SERF and other ultra-sensitive atomic magnetometers.

1 Introduction

In this chapter, we will review the most sensitive high-density atomic magnetometers (AM) and some of their multiple possible applications. The most notable feature of these magnetometers is that they exceed fT sensitivity [1] without requirements for

I.M. Savukov (✉)
Los Alamos National Laboratory, Los Alamos, NM, USA
e-mail: isavukov@lanl.gov

cryogenic cooling. Currently AMs can compete with SQUIDs in many applications that require the highest possible sensitivity. Magnetoencephalography (MEG) has become the primary target application, since the AMs are the only non-cryogenic alternative to SQUIDs [2–4]. Other applications include ultra-low-field (ULF) MRI [5] and ULF NMR [6, 7], which hold promise to revolutionize magnetic resonance; magneto-cardiography (MCG) [8] and biomagnetism in general. Submarine detection and space magnetic field measurements [9] are important national security applications. AMs provide many advantages because they are both relatively sensitive compared to conventional inexpensive magnetometers, such as fluxgates, and more convenient and less restrictive compared to SQUIDs. For several decades low-Tc SQUIDs had been by far the most sensitive magnetometers at low frequency, but the situation has now changed.

We will focus on discussion of the spin-exchange relaxation-free (SERF) atomic magnetometer [10] and its derivatives including high-density radio-frequency (RF) [6] and scalar magnetometers [11]. Because spin-exchange (SE) cross-section exceeds other relaxation cross-sections by orders of magnitude [10], the SERF magnetometer in which SE effects are eliminated [12] has superior sensitivity, better than fT/Hz$^{1/2}$ [1, 13]. Thus the key to the SERF and SERF-derivative magnetometers is the understanding of SE effects, which are covered in this chapter. Apart from the SE aspect, several properties of SERF and SERF-like magnetometers are important to consider: the high density of atoms and hence high temperature of the atomic cell, the use of buffer gas to prevent collisions with the walls, and the two-beam pump-probe scheme, which can be reduced to a less-sensitive single beam scheme.

1.1 SERF Magnetometers

Spin-exchange-relaxation-free (SERF) magnetometers have the potential for the highest possible sensitivity [1, 10, 13]. To reach the SERF regime and sub fT sensitivity for a cm-size vapor cell, a certain atomic spin density for a given field is required, actually on the order of 10^{14} cm^{-3} as found experimentally. For atomic magnetometers, such densities are considered high, so for this reason they can be referred to as high-density AMs. Any alkali-metal atom can be used, but K, Rb, and Cs are most practical and convenient. K SERF gives the highest sensitivity, but needs the highest operating temperature −180 °C; Cs has the lowest sensitivity and requires the lowest temperature (100–120 °C); Rb occupies the place in between. The high temperature of operation is the main disadvantage of SERF magnetometers, mostly due to issues related to oven design, such as compromise in heating methods and limited choice of non-magnetic, non-conductive materials structurally stable at required temperatures. In this regard constructing ovens for K cells is the most demanding task. Important consideration is the long-term deterioration in cell performance when it is heated to elevated temperatures.

Initially, SERF magnetometers relied on hot air heating [10] to minimize magnetic field noise, and the system consisted of a heating element, a copper or high-temperature plastic tube connected to a source of compressed air, a double-wall oven with vacuum-tube inserts as windows for light. A high-temperature non-metalic oven, together with the tube, was surrounded by a thick layer of thermal insulation. A long tube, the short path of air in the oven, and exhaust of hot air from the oven resulted in excessive heat losses and hence low power efficiency. A bulk of the oven is an additional negative factor. Electrical power for heating was as high as 1 kW, with extra power reserve required for fast heating and accurate temperature control. This heating system was also rigid, suitable mostly for lab applications with a magnetometer positioned inside a shield. So it is not surprising that an alternative was actively sought. Later on, air heating was replaced with electrical heating, which dramatically reduced the oven size and power consumption [14]. But the electrical heating introduced other problems, such as Johnson noise and low duty cycle. To reduce Johnson noise in the AM, the heating element was positioned at some distance from the cell and electrical current was switched off during measurement. In addition to creating noise, the magnetic field from the electrical heater perturbed atomic polarization, and to mitigate this, a high-frequency AC current has been used to which atomic spins do not respond [15]. In spite of the shortcomings, the electric oven design is invaluable in out-of-the-lab applications, where power consumption and portability are at premium and became commonly adopted by many groups. An alternative laser heating method became practically possible in an AM with a small Rb cell [4]. But this type of heating has its own drawbacks when applied to 1-cm cells [16], such as possibility of burning the light-absorbing material used to convert light to heat.

Returning to the discussion of the choice of an optimal alkali-metal atom, one criterion is the fundamental sensitivity or quantum noise. As we will show later, in the SERF regime the fundamental noise depends on the spin destruction (SD) (spin-de-coherence) rate as $R_{SD}^{1/2}$. In the sequence of K, Rb, Cs, which has the spin destruction rates in ratios 1:10:100 [10, 17, 18], the fundamental sensitivities scale as 1:3:10, and even the least sensitive Cs SERF magnetometer is expected to have fundamental noise on the order of 0.1 fT/Hz$^{1/2}$, better than the demonstrated sensitivity level with a potassium cell, 0.16 fT/Hz$^{1/2}$ [13]. The fundamental sensitivity limits currently are well below the demonstrated sensitivities, which are limited by technical noise, and for applications in the presence of magnetic field noise of a few fT, for example due to thermal currents in the magnetic shield, it seems that K, Rb, and Cs are all good choices for AMs. The demonstrated sensitivities is the highest for K [1, 13]; Rb SERF occupies the second place with demonstrated sensitivity of a few fT [3]; Cs SERF comes the last, with demonstrated sensitivity of 40 fT (4 fT photon-shot noise level) [19]. The advantage of low temperature of Cs cell was exploited for the detection of NMR in a microfluidic channel with a Cs SERF based on a microfabricated cell in [20].

Important motivation for developing atomic magnetometers comes from "outdoor" applications, in which portability, low weight, low-power consumption, and

vibration stability are essential. The first SERF magnetometer [1, 10] was implemented on a special non-magnetic optical table with a multi-layer mu-metal shield reducing the ambient magnetic field by a factor of 1 million, and due to the complexity of experimental arrangement and high price, such magnetometers would have only limited use, in the lab with the aim to demonstrate the highest possible sensitivity or in fundamental experiments. For external applications the design had to be simplified and miniaturized, and for successful commercialization, the price also had to be greatly reduced.

With the goal of cost and weight reduction, Kitching's NIST group has been working on the micro-fabrication of miniaturized atomic vapor cells and the integrated laser-electronics packaging, a spin-off project from miniature atomic clock development [14, 21]. They showed that the clock package can be adapted to magnetic field measurements with sensitivity of 50 pT/Hz$^{1/2}$ at 10 Hz. The clocks/magnetometer modules consisted of many layers of various functional components: lasers, filters, lenses, quartz waveplates, ITO heaters, atomic cells, and photodiodes. The components, thin wafers, were stacked on the top of each other to form a compact assembly. Because magnetometers of this type initially were not set up in the SERF configuration, they had fairly poor sensitivity. However, when in a follow-up experiment, a microfabricated atomic cell was tested in the SERF regime, dramatic improvement in sensitivity, almost 1000 times, to the level of 65 fT/Hz$^{1/2}$ was observed [22]. Even higher sensitivity should be possible from the analysis of fundamental quantum noise. One problem with microfabricated cells is that they have significant spin-destruction rate due to diffusion to the walls, so the magnetic resonance is much wider than in a cm-size cells, but in principle this can be compensated by operating the cell at higher than normal temperatures [23].

In parallel at Princeton a cm-scale magnetometer with a small oven and optic setup has been tested to show a high sensitivity on the order of a few fT/Hz$^{1/2}$ [24]. The single-beam fiber-coupled design allowed for not only miniaturization but also flexibility. Indeed, later on, commercial prototypes based on fiber-coupling appeared [4, 25], and now high-sensitivity cm-size atomic magnetometers became commercially available.

The interest in high-density AMs was initially stimulated by high sensitivity in the SERF regime; however, later it was also shown that high-density AMs can be very sensitive outside the SERF regime [6]. For this reason, we combine the overview of SERF and other types of high-density magnetometers in one chapter. The qualitative difference between SERF and non-SERF high-density magnetometers is in the effects of SE collisions on spin de-coherence and sensitivity, so the SE phenomenon will be discussed in some detail.

1.2 Operating High-Density AMs Outside the SERF Regime

Typically the SERF magnetometer is operated with all fields precisely zeroed, and the magnetometer has its frequency sensitivity profile similar to that of the

first-order low-pass filter, with the bandwidth proportional to spin de-coherence rate. When the frequency f of the measured field is outside the bandwidth, the signal falls off as $1/f$ and the sensitivity is mostly lost above a few hundred Hz. The sensitivity can be partially restored if a bias field is applied to "tune" the magnetometer to the frequency of interest [6, 26]. When the resonance frequency exceeds the resonance width, the AM frequency response exhibits a distinct resonance with an additional tail coming from the oppositely rotating field component. At zero field, the contributions from the two resonances double the signal, but with a significant bias field, only one resonance contributes. However, more importantly, the bias field leads to the additional broadening from SE collisions, signifying operation outside the SERF regime. Initially, the SE broadening grows quadratically with the field, but then it slows down and reaches asymptotically some maximum value, which is a non-small fraction of the SE rate. The SE broadening, in addition to the bias field, depends on spin polarization and hence the pumping rate. At a high pumping rate, it is possible to suppress SE broadening with the process known as light narrowing [27]. Pumping, however, leads to additional spin-decoherence, so there is a minimal value of the resonance width, experimentally observed on the order of 100 Hz [6], at the optimal pumping rate, which depends on SE and spin-destruction (SD) rates. Because with frequency laser technical noise decreases and can approach the photon-shot noise limit, of ten nrad level at typical laser power used, it is possible to reach sub fT sensitivity for SE-affected wider magnetic resonances of several hundred Hz [6, 28]. We will discuss RF magnetometer sensitivity and light narrowing in more detail later (e.g. Eqs. 9 and 23).

The RF magnetometer can be converted to a scalar magnetometer if its resonance frequency, which is proportional to a bias magnetic field, is used to measure the field. The only complication is that the coefficient of proportionality, the gyromagnetic factor, is not constant and depends on other parameters. At low frequency it can change by a factor of 1.5 in the case of Rb-87 or K, when field and polarization vary [26]. At a high frequency below the hyperfine frequency, the gyromagnetic factor is almost constant, so the scalar magnetometer can give the absolute value of the field. Near and above the hyperfine frequency, the Zeeman splitting between different levels becomes noticeably unequal leading to distinct multiple magnetic resonances. These resonances can be observed in the Earth's field in atomic cells with low buffer-gas pressure and anti-relaxation coating, when resonance widths are smaller than the splitting. The consequence of multiple resonances is that magnetic field measurements based on resonance frequency will depend on orientation, resulting in the so-called heading error, which limits accuracy to 1–10 nT level. For measurements of the field on the fly, this can be a problem.

2 Principles of Operation and Theory

2.1 The Interaction of Spins with Magnetic Field

A typical high-density atomic magnetometer, such as SERF, contains a heated vapor cell filled with alkali-metal atoms. These atoms have unpaired electron spins which interact with magnetic field. By measuring spin states, one can measure the magnetic field. Quantum-mechanically, the interaction between an atomic spin and a magnetic field is described by the Hamiltonian

$$H = \gamma_e \mathbf{J} \cdot \mathbf{B} + \gamma_N \mathbf{I} \cdot \mathbf{B} + a_{hf} \mathbf{J} \cdot \mathbf{I} \tag{1}$$

Here $\gamma_e = g_J \mu_B / \hbar$, $\gamma_N = g_I \mu_B / \hbar$, μ_B is the Bohr magneton, g_J, g_I are electron's and nuclear g-factors, $\mathbf{J}$ is the total angular momentum of the electron, which is the sum of the electron spin and the orbital momentum, $\mathbf{J} = \mathbf{S} + \mathbf{L}$; $\mathbf{I}$ is the nuclear angular momentum, and a_{hf} is the hyperfine constant. This Hamiltonian is responsible for the splitting of degenerate m-sublevels in magnetic field, called the Zeeman splitting. The solution of Eq. (1) in the case of $\mathbf{J} = \mathbf{S} = 1/2$ is known as Breit-Rabi equation [29]:

$$W(F, M_F) = -\frac{\Delta W}{2(2I+1)} - \frac{\mu_I}{I} B M_F \pm \frac{\Delta W}{2} \sqrt{1 + \frac{4M_F}{2I+1} x + x^2} \tag{2}$$

where $\Delta W = a_{hf} [F_2(F_2+1) - F_1(F_1+1)]/2$ is the hyperfine splitting between $F_2 = I + 1/2$ and $F_1 = I - 1/2$ states at zeros field, $x = (g_J - g_I)\mu_B B / \Delta W$, $g_I = -\mu_I / I\mu_B$. Table 1 gives the list of parameters for different isotopes that can be used in atomic magnetometers. Figure 1 shows a typical dependence of the energy of hyperfine sublevels on applied magnetic field. The transitions between magnetic sublevels $M \rightarrow M \pm 1$ can be induced by time-varying magnetic field that leads to the interaction Hamiltonian $H_{\text{int}} = \gamma_e \mathbf{J} \cdot \mathbf{B}(t) + \gamma_N \mathbf{I} \cdot \mathbf{B}(t)$. The Zeeman resonances often have the Lorentzian shape with the width determined by the spin decoherence rate. Multiple resonances at a low field have almost the same frequency for a given field; however, in a large field the frequency degeneracy is removed, and multiple resonances can be observed. The resonance frequency is the function of the applied dc field and can be used to measure the absolute value of the magnetic field or with higher sensitivity its relative variation.

| Table 1 Parameters for calculating Breit-Pauli splitting; μ_N is the nuclear magneton	Alkali-metal atom	I	ΔW (MHz)	μ_I / μ_N
	^{39}K	3/2	461.7	+0.39147
	^{41}K	3/2	254.0	−0.21487
	^{85}Rb	5/2	3036	+1.3527
	^{87}Rb	3/2	6835	+2.7506
	Cs	7/2	9193	+2.578 8
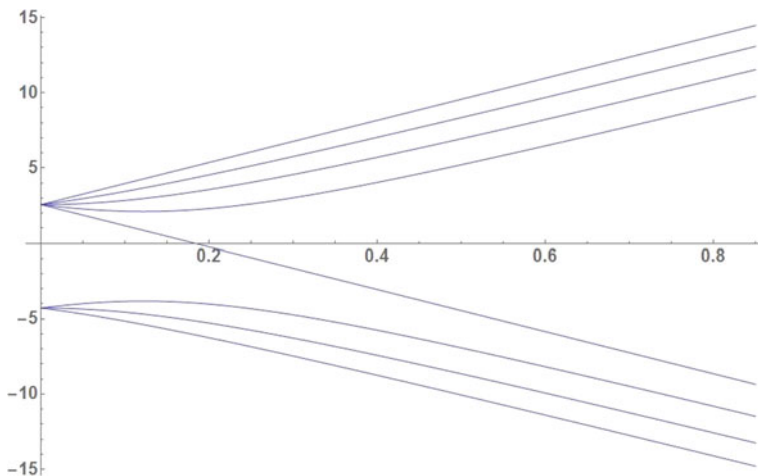
Fig. 1 Zeeman splitting in GHz as a function of magnetic field in T for the case of Rb-87, I = 3/2

2.2 Light-Spin Interactions

There are at least two methods for creating significant spin polarization: (i) application of magnetic field and (ii) irradiation of atoms with resonant circularly polarized light [30]. For the first method, to reach high degree of polarization would require prohibitively large fields, not to mention that such fields or coils generating them would interfere with sensitive measurements; thus, the field-polarization method is impractical for use in atomic magnetometers. The second method—*optical pumping*—is not only very efficient but also straightforward to implement. Not surprisingly, all sensitive atomic magnetometers rely on this second method. How does optical pumping work? Intuitively, optical pumping can be understood from the conservation of angular momentum, since with the absorption of a photon, a unit of angular momentum is transferred to the atom. The conservation of angular momentum, on the other hand, is the consequence of the well-known m-selection rules. Using these rules, the pumping efficiency can be predicted if we also consider the balance between various transitions in the atom after it absorbs a photon. In the presence of buffer gas, usually added to the alkali-metal cell of high-density AMs, in a quantity of 1 amg or so, the hyperfine levels are not resolved, and only four levels (Fig. 2) will be necessary to consider: two m-sublevels of the ground state and two m-sublevels of the $p_{1/2}$ excited state. Note that for simplicity and practical relevance we consider here the pumping on the D1 line: Other lines can be used as well, but pumping on the D1 line is most optimal for achieving almost 100 % polarization in optically dense vapor. When a circularly polarized photon is absorbed, an alkali-metal atom undergoes the transition $|ns_{1/2}, -1/2\rangle \rightarrow |np_{1/2}, +1/2\rangle$, which depletes the population of the $-1/2$ ground state. If the atom returned to the same state, no pumping would occur, but because of fast collisions with nitrogen

Fig. 2 Diagram for
explaining depopulation
pumping with a circularly
polarized light with a
four-level system
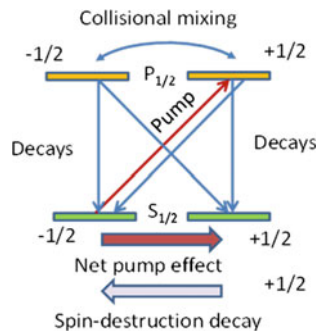
molecules (added to improve pumping efficiency) equally repopulating the excited
states and following radiative transitions to the both ground states with equal
probability, the transfer of population from the $-1/2$ ground state to the other ground
state will be significant. The pumping efficiency, as measured by the ratio of the
number of polarized atoms to the number of absorbed photons, is quite high, only
somewhat reduced by the decays to the $-1/2$ ground state. More specifically, when
collisional mixing is faster than radiation decay, one absorbed photon would remove
one atom from the $m = -1/2$ ground state which then would return with equal
probability to either ground states, so the efficiency is one half of the case when the
atom would only return to the $m = +1/2$ state.

Optical pumping continuously creates difference in the population of Zeeman
sublevels, but the population is also randomly redistributed with some rate,
spin-destruction rate, due to various relaxation processes. After many
absorption/decay cycles, some equilibrium polarization, often close to 1, is estab-
lished, $R/(R + R_{SD})$, where R_{SD} is the spin destruction rate and R is the pumping
rate.

When spins are polarized, their dynamics can be described by a single average
spin. In a magnetic field, it will change its orientation and magnetic field can be
detected by measuring one projection of the spin. For this, the rotation (the Faraday
effect) of the linear polarization by atomic vapor of the probe beam can be used.
The best sensitivity can be achieved when the probe beam is sent at the perpen-
dicular direction to the pump beam.

Optical probing is a highly sensitive method to detect the states of atomic spins
based on strong spin-dependent interaction of light with polarized atoms. This is for
two reasons. First, interaction of light with atoms is spin-dependent due to the
m-selection rules; second, the noise of polarization measurements is very low,
limited by the fundamental photon-counting noise of nrad level. Absorption mea-
surements are also possible, but they result in lower sensitivity. One drawback of
the absorption method is stronger decoherence of spins by light tuned closer to the
absorption resonance.

The absorption and Faraday rotation for a typical density of alkali-metal atoms
can be estimated by employing a two-level model, applicable to an atom colli-
sionally broadened in 1 amg of helium or nitrogen, which is a typical pressure in

high-density AMs. In this case, the collisional width exceeds both the Doppler width and the hyperfine splitting; thus the absorption coefficient is:

$$\alpha(v) = ncr_e f \frac{\gamma}{(v - v_0)^2 + \gamma^2} \tag{3}$$

Here n is the density of atoms, c is the speed of light, r_e is the classical electron radius, v is the frequency of light, f is the oscillator strength, and γ is the absorption profile linewidth. The maximum absorption will be in the center, $\alpha(v_0) = ncr_e f / \gamma$. When the potassium cell is filled with He, the linewidth is about 7 GHz (HWHM) or 0.014 nm per 1 amg (1 amg is the density of the gas at normal conditions) [26]. This line width at He density on the order of 1 amg exceeds the hyperfine spitting of ^{39}K (I = 3/2), 462 MHz, and the Doppler width HWHM = 500 MHz. In heavier alkali-metal atoms the hyperfine splitting, which is 3036 MHz in Rb (I = 5/2) and 9192 MHz in Cs (I = 7/2), can become comparable to the buffer gas broadening at 1 atm and more complicated model needs to be used.

In the Faraday detection method, the probe laser is detuned from the resonance, which facilitates the propagation of light through the optically thick medium and reduces the spin destruction by the probe light, which follows the profile of $\alpha(v)$. Linearly polarized light can be decomposed into two circularly polarized components, and because refractive indices n_+ and n_- are not equal due to differences in the population of the m-sublevels (this is when spins are polarized), the plane of polarization of linearly polarized light will be rotated by non-zero angle

$$\theta = \frac{\pi(n_- - n_+)l}{\lambda} \tag{4}$$

Here λ is the wavelength and l is the pathlength. Large rotation of light polarization in optically pumped vapors is due to the strong dependence of the refractive index on atomic spin orientation. It can be derived from Eqs. 3–4 and the Kramers-Kronig relations that the rotation angle by alkali-metal atoms is

$$\theta = \pm \frac{1}{2} l r_e cfn P_x D(v - v_0) \tag{5}$$

where $D(v)$ is Lorentzian dispersion profile, $D(v) = \frac{v}{v^2 + \gamma^2}$. The rotation for D1 and D2 lines are of opposite signs. In most practical cases, only one line needs to be considered.

While optical pumping leads to redistribution of populations, both the pump or probe beams can affect the Zeeman splitting, similarly to magnetic fields. The effect is referred to as light shift. The pump rate R and light shift L are both proportional to the intensity of the circularly polarized light, and they can be found from the expression for the complex optical pumping rate:

$$R + iL = \pi r_e c f \Phi \Lambda(v - v_0) \tag{6}$$

where $\Lambda(v) = \frac{1}{2\pi} \frac{2\gamma + iv}{v^2 + \gamma^2}$ and $\Phi = I/hv$ is the photon flux.

It can be immediately seen that light shift is comparable to the pumping rate when the light is detuned by one linewidth from the absorption maximum. Light shift follows the dispersion Lorentzian, while the pumping rate follows the absorption Lorentzian, with the same coefficient. Divided by gyromagnetic factor, light shift will have units of a magnetic field and it can be included into the Bloch equations or in the density matrix equation as an additional fictitious magnetic field. Its direction coincides with the direction of the laser beam and the sign depends on the sign of circular polarization. Normally, only circularly polarized light creates light shift. When light is linearly polarized, it consists of almost equal number of circularly polarized photons of two signs, with small fluctuation in the difference. The fluctuations lead to so-called light-shift noise [6].

For elliptically polarized light, in general, it can be written that

$$P = \mathbf{s} \cos \theta R / (R + R_{SD}) \tag{7}$$

where $\mathbf{s}$ is the vector which amplitude is equal to the degree of circular polarization and direction is pointing along the pumping beam direction. Scattering of pump light by atoms can lead to pumping in "wrong" directions and the reduction in the polarization. To minimize the scattered light from re-emission, the AM cell is filled with nitrogen buffer gas that effectively quenches excited states faster than the radiation decay.

Since the light intensity and frequency constantly fluctuate and the intensity is not uniform across the AM cell, light shift both adds noise to the AM signal and broadens magnetic resonances similarly as magnetic field gradients. If intensity fluctuations play a dominant role, the light shift effects can be minimized by tuning the laser to the center of the absorption resonance. If frequency fluctuations are more important, then light-shift noise can be minimized by detuning from the center, but in general it is impossible to remove completely light shift noise by changing the wavelength. Light shift produced by linearly polarized probe beam (probe light shift) can also lead to the noise and broadening, not only due to fundamental fluctuations in the number of photons, but also due to imperfections of glass cell windows and other optics that lead to birefringence. By stabilizing wavelength and intensity, the fluctuations in light shift can be reduced, so it is important to use high-quality lasers not only for probing but for pumping as well.

As we mentioned above, alkali-metal atoms have two strong D1 and D2 absorption lines in a convenient wavelength range, but the D1 line is preferable due to higher polarization level that can be achieved in optically dense vapors. One reason for this is that D1 light is less attenuated in optically dense polarized vapors. Actually, the intensity I of the D1 line follows this equation

$$dI/dz = -\alpha(1 - P_z)I \tag{8}$$

and intensity attenuation is substantially reduced when the polarization projection along the propagation direction P_z is close to 1. This is not true for the D2 line. Alternatively, to avoid strong absorption in an optically dense vapor, the pump laser can be tuned off the D1 or D2 resonance. For far enough detuning, the intensity attenuation can become linear with the propagation distance rather than exponential, and this would improve the uniformity of AM sensitivity across the cell, especially if a counter propagating beam is added by, for example, retro-reflecting the beam after it passes the cell. One consequence of detuning is large light shift. It can be minimized by having two frequencies on opposite sides of the center of absorption [28].

For probing, D1 also gives some advantage because of smaller absorption coefficient (note that the absorption reduces the probe beam intensity on the photo-diode and hence shot-noise sensitivity); still, D2 line has been used for probing in some cases for example to combine probe and pump beams in a single beam and separate them after the cell [3].

2.3 Spin-Exchange Collisions

SE collisions between alkali-metal atoms have cross-sections on the order of 10^{-14} cm^2, substantially exceeding the cross-sections of spin-destruction collisions [10]. In case of potassium, which is used in most sensitive SERF magnetometers, the ratio is very large, $\sim 10^4$. SE collisions can limit the sensitivity of AMs. Because alkali-metal atoms have a non-zero nuclear spin, the ground state is split in many sublevels each having its own somewhat independent evolution and interacting with others. For complete analysis, the density-matrix-equations (DME) have to be solved [10, 26] (a short discussion is provided below).

The SERF magnetometer idea is based on the discovery by Happer and Tang [12] that in a small magnetic field the spin-resonance lines at high densities of alkali-metal vapors become very narrow. Happer and Tam [31] derived an analytical expression for the frequency shift and width of magnetic resonances for an arbitrary SE rate in the limiting case of low polarization. This equation predicts zero broadening at large SE rates at zero field, essentially the SERF regime, although low polarization is not optimal for the SERF operation. Another interesting effect—light narrowing of magnetic resonances, or more precisely the reduction of the SE contribution to transverse relaxation rate at high polarization levels—was discovered much later in 1998 by Appelt et al. [27]. The analysis of SE effects at low magnetic field for an arbitrary spin polarization was first performed in [10], where it was shown that SE relaxation is completely eliminated at zero field for arbitrary spin polarization. The density-matrix equations that contain SE collisions, optical pumping, and other terms for complete description of the SERF magnetometer have been formulated in [10, 32]. The numerical solution of this density-matrix equation

for an extensive range of AM parameters, such as SE rate, pumping rate, and magnetic field, has been obtained and compared with experimental measurements to establish a firm basis for the analysis of SERF and other high-density AMs [26].

2.4 Classification of High-Density AMs (SERF, RF AM, and Scalar RF AM)

The SERF magnetometer exploits full suppression of otherwise large effects of SE collisions on relaxation for superior sensitivity, especially at the fundamental level. However, the operation in the SERF regime is limited to a low frequency and magnetic field range. By applying a bias field the frequency range can be greatly extended, so it is interesting to consider the operation of the high-density magnetometer beyond the SERF regime, when the bias magnetic field is no longer small. The investigation of the non-SERF regime of "the SERF magnetometer" was conducted in detail in Ref. [26], which resulted later in the discovery that at high frequency an AM can also have fT sensitivity [6].

One characteristic feature in operation outside the SERF regime is that SE collisions start to affect the magnetic resonance of the spins. As we mentioned, SE collisions have much larger cross section than SD collisions, and the broadening due to SE collisions can be on the order of several kHz at typical densities of alkali vapors used in SERF magnetometers, exceeding by orders of magnitude a typical SERF bandwidth of several Hz. Because in the AM the bandwidth and the signal amplitude are inversely related, the bandwidth investigation is central for the analysis of the sensitivity. The bandwidth of high-density magnetometers and the broadening due to SE were investigated in detail [26] experimentally and numerically by solving the DM equation. An example of comparison of simulations with experiment is given in Fig. 3.

Fig. 3 Broadening of magnetic resonance with the field. Adopted from [26]
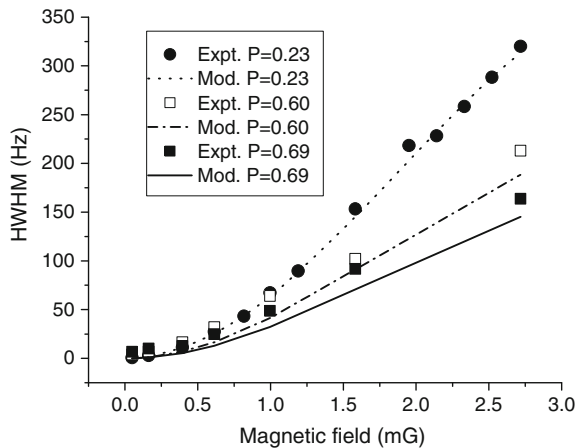
In the non-SERF regime, the SE broadening can reach levels of several kHz for typical SERF magnetometer operating temperatures. Good understanding of SE effects is essential for designing sensitive magnetometers at arbitrary frequency. For example, the SE broadening can be suppressed with light narrowing [27]. Light narrowing happens due to the reduction of the SE collisions between oppositely precessing spins of F = I + 1/2 and F = I − 1/2 hyperfine manifolds when the majority of atoms are populated into the stretched state (F = I + 1/2, M = F) by the strong pumping action. Additional detailed explanation is provided in Refs. [6, 26]. Experimentally, light narrowing of more than 10 times was observed, with similar improvement in magnetic field sensitivity. Although SE broadening can be totally suppressed by pumping all atoms into the stretched state, the pump light itself broadens the magnetic resonance, linearly with power, and thus an optimal pumping rate exists that minimizes the resonance width. This is evident from an analytical equation [6] in the limit of polarization close to 1:

$$T_2^{-1} = \frac{R}{4} + \frac{R_{SE}R_{SD}}{R} G(\omega_0, R_{SE}) \tag{9}$$

$$G(\omega_0, R_{SE}) = \mathrm{Re}\left[\frac{R_{SE} + 4i\omega_0^2/\pi v_{HF}}{5R_{SE} + 8i\omega_0^2/\pi v_{HF}}\right] \tag{10}$$

Here ω_0 is the spin precession frequency and v_{HF} is hyperfine frequency. This equation is derived for atoms with I = 3/2. In the case of precession frequency below the MHz range, $T_2^{-1} = \frac{R}{4} + \frac{R_{SE}R_{SD}}{5R}$ and the optimized pumping rate leads to the following minimal bandwidth: $(1/T_2)_{\min} = (R_{SE}R_{SD}/5)^{1/2}$. This width is much smaller than spin-exchange broadening in the no-light-narrowing regime, $R_{SE}/8$, because $R_{SD} \ll R_{SE}$, about 10,000 times in potassium. The light-narrowing factor, which is the ratio of the minimal width for the optimal pumping rate and the maximum width without light narrowing, is $K = (5R_{SE}/R_{SD})^{1/2}/8$. If the SD rate is dominated by K-K collisions, a condition that can be achieved by raising density of alkali-metal atoms, then $K = (5\sigma_{SE}/\sigma_{SD})^{1/2}/8$, where σ_{SE} and σ_{SD} are spin-exchange and spin-destruction cross sections. Potassium has $\sigma_{SE} = 1.8 \times 10^{-14}\,\mathrm{cm}^2$ and $\sigma_{SD} = 1 \times 10^{-18}\,\mathrm{cm}^2$, so the maximum light-narrowing factor $K_{\max} \approx 37$. In practice, such light-narrowing is hard to achieve due to, for example, non-uniformity of the pumping rate across the cell.

The high sensitivity of the RF magnetometer is achieved by bias field magnetic resonance tuning, light narrowing, and technical noise reduction at high frequencies. It turns out that in terms of demonstrated sensitivity the FR AM [6, 28] can be comparable to that of the SERF magnetometer [1, 13], primarily due to the latter technical noise limitations. The fundamental noise of the RF magnetometer has been investigated in Ref. [6]. We discuss this question in a separate section below.

Because the RF magnetometer sensitivity exhibits resonant behavior with resonance frequency being a function of the bias magnetic field, this magnetometer can be converted to a scalar magnetometer by applying an RF modulation field near
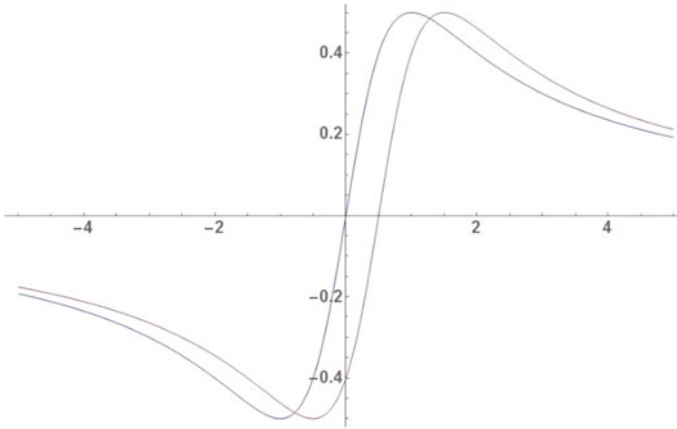
Fig. 4 Conversion of the RF magnetometer out-of-phase signal to the scalar magnetometer signal. Magnetic field shifts the curve and hence the RF signal is sensitive to the field. Arbitrary units are used, with the position of the maximum being on the order of magnetic resonance width

the resonance frequency, $\omega_L = \gamma \sqrt{B_x^2 + B_y^2 + B_z^2}$. Note that the position of magnetic resonance depends on the total field, not its projection. One advantage of the scalar magnetometer is that it can measure magnetic field in the Earth-field environment, without mu-metal shielding or field compensation, unlike the SERF. The resonance frequency is about 350 kHz (I = 3/2 atoms), and small variations in the Earth's field can be readily observed as the shifts in the resonance. The in-phase and out-of-phase lock-in amplifier signals near the magnetic resonance have absorption and dispersion Lorentzian dependencies on frequency. It is convenient to use the dispersion component that gives the maximum slope at the resonance (Fig. 4). Then the signal of the scalar magnetometer is proportional to the deviation of the field from the resonance condition. The lock-in amplifier can be used to demodulate the high-frequency RF magnetometer signal to extract slow-varying quasi-dc field. The sensitivity to the dc field is determined by the slope of the dispersive component. The slope of the RF magnetometer was investigated in Ref. [11]. Because the signal initially grows with the RF field excitation amplitude and then decreases due to SE broadening, optimal excitation amplitude exists. The fundamental limit of the sensitivity of the scalar magnetometer can be derived from that of the RF magnetometer in which the effects of large-excitation amplitude broadening are incorporated. The fundamental noise of the scalar magnetometer is investigated in a separate section.

The principal advantage of the scalar magnetometer is its insensitivity to orientation and possibility to operate in the ambient Earth's field without compensation coils. The scalar magnetometer can also measure the absolute value of the field without calibration by converting frequency to the field using the gyromagnetic constant. Unfortunately, the gyromagnetic constant slightly depends on the field,

polarization, and orientation, which is the consequence of multiple partially over-lapping Zeeman resonances. If the nuclear spin were zero, only one resonance would exist and its position would be a function of magnetic field only. In this regard, the He magnetometer has an advantage.

2.5 Dynamics of Atomic Spins

Spins in atomic vapors can have complicated dynamics. Their behavior is affected by magnetic fields, light-atom interactions, atomic-wall and interatomic collisions, and other factors. In the presence of spin-affecting collisions, the Schrödinger equation has to be replaced with the density matrix equations. In SERF and similar high-density magnetometers, only ground-state hyperfine sublevels need to be considered. There are $2F + 1 = (2I + 2)$ upper and $2I$ lower hyperfine states with the total number of $4I + 2$ states (in the case of I = 3/2, 8). Zeeman splitting at low field is linear and the hyperfine states oscillate with the same frequency in magnetic field (recall that ac magnetic field causes transitions between neighboring M states), although the precession directions of spins of the lower and upper hyperfine states are opposite. Spin exchange collisions strongly affect the evolution of hyperfine sublevels. However, SE collisions conserve the total angular momentum of the colliding pair, and at certain conditions, when AM operates in the SERF regime, SE collisions do not lead to change in the polarization and do not affect the coherence. Qualitative and intuitive considerations are possible, but ultimately to simulate spin dynamics and extract important parameters such as the magnetic resonance width, the density matrix equations need to be solved. The density matrix equations provide accurate description of the system, as long as experimental parameters such as spin density, buffer gas pressure, laser intensities and polarization are specified.

2.5.1 Density Matrix Equations

The behavior of atomic spins in alkali-metal vapors is quantitatively described with the following density matrix (DM) equation [10, 26, 32, 33]:

$$\frac{d\rho}{dt} = a_{hf}\frac{[\mathbf{I}\cdot\mathbf{S},\rho]}{i\hbar} + \mu_B g_S\frac{[\mathbf{B}\cdot\mathbf{S},\rho]}{i\hbar} + \frac{\varphi(1+4\langle\mathbf{S}\rangle\cdot\mathbf{S}) - \rho}{T_{SE}}$$
$$+ \frac{\varphi - \rho}{T_{SD}} + R[\varphi(1+2\mathbf{s}\cdot\mathbf{S}) - \rho] + D\nabla^2\rho. \tag{11}$$

Here ρ is the density matrix, which has dimension of the number of hyperfine states; $\varphi = \rho/4 + \mathbf{S}\cdot\rho\mathbf{S}$ is the pure nuclear part of the density matrix, $\langle\mathbf{S}\rangle = Tr(\rho\mathbf{S})$, T_{SE} is the spin-exchange collision time, T_{SD} is the spin-destruction time, R is the pumping rate, and $\mathbf{s}$ is the optical pumping vector defined earlier. The first and the second terms describing the hyperfine and Zeeman interactions are

obtained from the Von Neumann equation, $i\hbar\frac{d\rho}{dt} = [H, \rho]$, where H is the Hamiltonian defined in Eq. 1. The rest are spin-exchange, relaxation, optical pumping, and diffusion terms. The solution of the DM equation can be used to explain many observed effects in atomic magnetometers, including the spin precession frequency and decoherence rate in a wide range of experimental conditions. The DM equation is considered the most appropriate theoretical framework, but, unfortunately, in many cases only numerical solutions are possible. Note that the SE term, $\frac{\varphi(1 + 4\langle \mathbf{S}\rangle \cdot \mathbf{S}) - \rho}{T_{SE}}$, is non-linear, and the solution using eigenvalue-finding subroutines is not immediately applicable. Instead, an iterative solution has to be used with appropriate zero-order guess solutions. Under some conditions, the DM equation can be simplified and analytical solutions can be derived. It is also quite useful to separate the expectation value of spin into two parts, averaged over the upper (F = I + 1/2) $\mathbf{S}_{up}$ and the lower (F = I − 1/2) $\mathbf{S}_{down}$ hyperfine manifolds of the ground state. At low field, the spins of these manifolds rotate with equal but opposite frequency:

$$\frac{d\mathbf{S}_{up}}{dt} = \gamma \mathbf{B} \times \mathbf{S}_{up}$$
$$\frac{d\mathbf{S}_{down}}{dt} = -\gamma \mathbf{B} \times \mathbf{S}_{down}$$

$$(12)$$

If the density were small, these two groups would precess independently, but at typical densities of SERF magnetometers, the strong SE interaction affects their dynamics. In the SERF regime, when between SE collisions the spins of the two manifolds do not significantly change orientations, they tend to rotate together, but at slower rate. In non-SERF regime, the spins of the two manifolds start to spread, and after SE realignment, transverse polarization becomes lost. When pumping is strong enough to populate most spins into the stretched state, the RF magnetometer would have much smaller number of atoms in the down manifold, resulting in the reduced spin-decoherence rate from the SE collisions.

When no field excitation is applied, SE collisions lead to establishing the well-known in NMR spin-temperature (ST) distribution:

$$\rho_{ST} = k_n \exp(\boldsymbol{\beta}\mathbf{F}) \tag{13}$$

where $\boldsymbol{\beta}$ is the ST parameter, k_n is the normalization factor, and $\mathbf{F}$ is the total angular momentum vector. This specific matrix is the eigensolution of the DM equation that contains the SE term.

The ST distribution for I = 3/2 is illustrated in Fig. 5. The ST distribution is maintained in the SERF regime in the static and the rotating frame, if the spin precession is induced. Outside the SERF regime, the ST distribution is not valid, but when the deviation from the SE distribution is small, perturbation theory can be effectively used to obtain a solution. The dynamics of spins in the RF AM was analyzed with this approach [6, 26, 33].

Fig. 5 A typical spin-temperature distribution for the case of I = 3/2
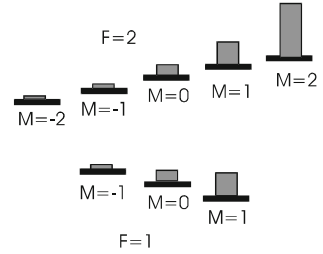
Fig. 6 Dependence of the gyromagnetic factor on spin polarization. Adopted from [26]
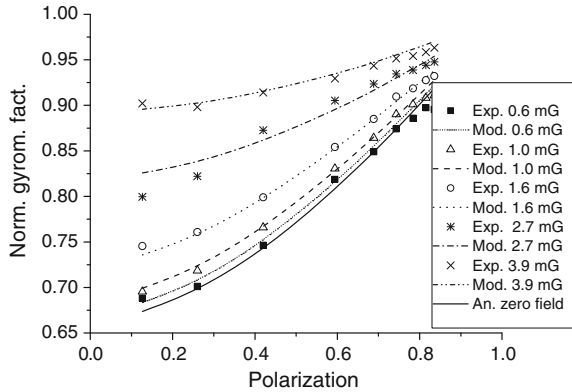
The solution of DM in the general case was analyzed and compared against experimental data in [26]. For example, it was found that gyromagnetic factor depends on the field and polarization as shown in Fig. 6. The magnetic resonance width also depends on these parameters (Fig. 3).

2.5.2 Bloch Equation

In the SERF regime, because the spins precess with the same frequency and relax with the same rate, they can be described by a single Bloch equation:

$$dS_x/dt = \gamma S_y B_z - \gamma S_z B_y - S_x/T_2$$
$$dS_y/dt = -\gamma S_x B_z + \gamma S_z B_x - S_y/T_2 \tag{14}$$
$$dS_z/dt = \gamma S_x B_y - \gamma S_y B_x + (S_0 - S_z)/T_1$$

Here γ is the gyromagnetic ratio of atomic spins, T_1 is the longitudinal relaxation time, and T_2 is the transverse relaxation time. This behavior can be verified by direct solution of the DM equation. Outside the SERF regime but when spins are fully polarized, the behavior of spins can still be described with one Bloch equation. The effect of the spins from the down manifold precessing in the opposite direction can be incorporated into modification of the gyromagnetic factor and relaxation

rates. The rotating frame approximation, which is often used for deriving analytical solutions of the Bloch equation, can be applied, as long as the interaction with the down-manifold spins can be neglected beyond their contributions to the gyromagnetic factor and relaxation constants.

The description of dynamics with the Bloch equation is convenient to exploit the analogy with NMR [34], where it is the basis for the analysis of a multitude of sequences for manipulating nuclear spins. Among topics that can be readily studied by analogy with NMR are: the free-induction decay, spin echo, spin-temperature distribution, motional narrowing, broadening by the RF field and field gradients, validity of rotating wave-approximation, magnetic-resonance imaging. Even when the Bloch equation is not strictly applicable, it can still provide qualitative guidance for many experiments with atomic magnetometers. For example, a small excitation amplitude solution of the DM equation for a given separate resonance is equivalent to a small amplitude solution of the Bloch equation. This becomes evident with the use of complex variables $A_+ = A_x + iA_y$ allowing us to simplify the Bloch equation to this form:

$$dS_+/dt = i\gamma(B_z S_+ - S_z B_+) - S_+/T_2 \tag{15}$$

In the SERF regime, a steady-state solution of the Bloch equation can be used to characterize the dynamics of spins and obtain the magnetometer signal:

$$S_x = S_0 \frac{\gamma B_y T_2 - (\gamma T_2)^2 B_x B_z}{1 + (\gamma T_2)^2 (B_x^2 + B_y^2 + B_z^2)} \tag{16}$$

In this equation, T_2 includes the broadening by the pump beam. The x-component of the spin, which is along the probe beam, gives normally the signal of the SERF magnetometer that has orthogonal pump and probe beams.

2.5.3   Tuning Fields for Maximum Sensitivity

According to Eq. 16 to maximize the sensitivity of the SERF magnetometer all magnetic-field components have to be zeroed. There are several strategies for doing this. In one strategy, the dc AM signal offset is used to zero the By field, then Bx is modulated to zero the Bz field, and Bz is modulated to zero the Bx field. The process is repeated until convergence is achieved. An alternative strategy is to maximize the signal induced by low-frequency By modulation by varying all three components in an arbitrary sequence. This strategy works because the denominator containing the sum of squares of all the components is minimized independently when each component is zeroed. The modulation frequency has to be lower than the bandwidth for the steady-state solution to be valid. If frequency is too high, the signal maximization procedure can result in some residual non-zero field. This is because outside the steady-state regime, the resonance enhancement for a non-zero

bias field would increase the signal. In the presence of noise, using high-frequency magnetometer signal can be useful for approximate zeroing of transverse components.

Apart from giving maximum signal, field zeroing also helps to reduce light-shift noise that can be present due to pump and probe laser frequency and intensity fluctuations. Light shift is equivalent to magnetic field, as we discussed earlier, and the SERF signal will depend on the product of Bx and Lz, where Lz is the light shift along the pump direction. Similarly, the contribution of the probe light shift noise will be proportional to Bz, and it can be removed by zeroing Bz.

When a magnetometer is tuned with a biased field and its operation moves outside the SERF regime, the situation become quite different. First, zeroing all components is replaced with zeroing transverse components only. The AM response to Bx and By fields is the same, and the AM output can be maximized using the modulation of either component. Second, RF AM would have the light-narrowing effect maximized when the total field is along the pump direction, and hence by maximizing the output, the transverse components will be zeroed. Because when the transverse components are smaller than the z component, their effect on frequency is quadratically small, the iterations of maximization by adjusting transverse and then longitudinal components would converge. The pump light-shift noise becomes suppressed when the transverse fields are zeroed, but probe light-shift noise does not. Thus it is important to have a probe laser with a stable amplitude and frequency, also its beam expanded to reduce the light intensity and hence the magnitude of light shift.

Tuning the fields for the scalar magnetometer is not discussed in the literature. To some extent, the scalar magnetometer by definition has to be immune to field orientation. Apparently, if it is based on the RF magnetometer, the performance of the RF magnetometer has to be optimized. However, there could be some additional issues with the scalar magnetometer. Pump light-shift becomes very important to consider and its contribution to the signal cannot be removed by adjusting fields. The probe light shift plays a similar role as in the RF magnetometer.

Finally, the fields in a parallel beam SERF magnetometer [3, 24] can be zeroed as well using the signal maximization strategy discussed above. The steady-state solution for the z component can be similarly derived from the Bloch equation.

2.5.4   Analogy with NMR

Atomic spins obey the Bloch equation under some conditions (SERF regime; strong polarization case) as nuclear spins and direct analogy with NMR exists that can be exploited. The field of NMR is very rich, including applications of many pulse sequences, such as free induction decay (FID), spin-echo, Car-Purcell-Meiboom-Gill (CPMG); this analogy can be used for benefits of both NMR and atomic magnetometry. Some work has been already done, merely scratching the surface, but a lot remains to be explored. To give some flavor of possibilities, below we will discuss magnetic resonance imaging of Rb-87 spins.

2.5.5 Magnetic Resonance Imaging of Rb Atomic Spins

Magnetic resonance imaging (MRI) is an extremely valuable method of imaging based on the precession of spins in a magnetic field. Introduction of MRI for medical diagnostics revolutionized the field. Many applications have been developed over the years. From the analogy between nuclear and alkali-metal spins, which includes a similar resonance response to the RF excitation in a magnetic field, long coherence times, possibility for frequency and phase encoding with constant and pulsed gradients, it is obvious that MRI methods can be used in experiments with atomic spins. Several publications have demonstrated MRI of Rb and Cs spins. Below we will describe in some detail an imaging experiment published in [34].

As in usual MRI, the system contains uniform-field and gradient coils; the uniform field is necessary to specify the spin precession frequency, while gradients are used for frequency and phase encoding. The field strength is much below the field in conventional MRI, but considering much larger polarization of the atomic spins achieved with optical pumping and high-sensitivity of optical detection, the low-field operation should provide sufficient SNR.

A 3D MRI gradient-echo method with one frequency and two phase-encoding gradients was used to image the polarization in the atomic cell. The sequence started with a $\pi/2$ pulse, which excited polarized Rb-87 spins. During the $\pi/2$ pulse all gradients were off to avoid the slice selection or position-dependent phase accumulation. The gradient echo was formed by the reversal of the gradient G_z along the readout direction, which was also the direction of the pump beam. Phase encoding gradients G_y (the y axis approximately coincides with the probe-beam direction) and G_x were applied between the $\pi/2$ pulse and G_z reversal times, $t_{\pi/2}$ and t_{-G_z}.

The resulting image shown in Fig. 7 demonstrates resolution on the order of 1 mm. While in conventional MRI proton spins do not move much across the tissue, in the case of Rb spins, a characteristic diffusion length is comparable to the resolution. To reduce motional artifacts, the sequence timing was shortened to the
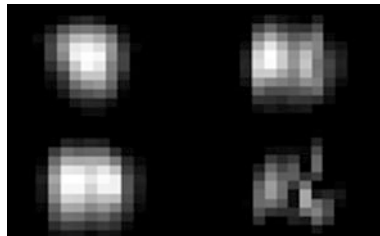
Fig. 7 Rb polarization in an atomic cell. Slices in depth are arranged from top to bottom and left to right in increments of 1.4 mm. In-plane resolution is 1.2 (horizontal) by 0.8 (vertical) mm^2. Resolution in vertical direction is affected by diffusion. The maximum brightness corresponds to polarization of 1. Adopted from [34]

Fig. 8 Polarization detection with a polarizing beam splitter (PBS)
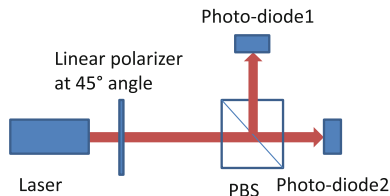
msec scale. One noticeable feature that some areas on the image of the atoms inside the cell are dark, meaning incomplete fill with pump and probe beams of the cell volume. Since the sensitivity depends on active volume, MRI of the magnetometer cell can be a valuable diagnostic tool for checking the beam alignment or for other troubleshooting tasks. More generally, MRI can be a valuable research tool for studying spin dynamics and interactions in the cell.

2.6 Polarization Rotation Measurement Schemes

Optical detection of the atomic spin state is normally based on the measurement of polarization rotation using laser polarimetry. A typical polarimeter consists of a polarizing beam splitter (PBS) and a polarizer rotated at an angle ($\sim 45°$) with respect to the PBS axis (Fig. 8). The intensities of the split beams are $I_0 \cos^2 \theta$ and $I_0 \sin^2 \theta$, where θ is the angle between light polarization and the axis of the beam-splitter cube. When the PBS outputs are accurately balanced, the noise arising from laser intensity fluctuations will be suppressed, in some cases 100 times. The angle rotation can be determined as

$$\delta\theta = \frac{U_1 - U_2}{2(U_1 + U_2)} \approx \frac{\delta U}{4U_1} \tag{17}$$

where U_1 and U_2 are the outputs of the two photo-detectors, usually measured with trans-impedance amplifiers. The noise level is determined by the number of electrons, which is the current divided by the electron charge.

An alternative polarimetry setup contains two crossed polarizers, a polarization modulator inserted between, and a photodiode. The signal is detected as the first harmonics of the modulation frequency. A polarization modulator reduces noise arising from intensity fluctuations in the probe beam and from other causes, which often inversely scale with frequency, 1/f noise. The modulation amplitude of polarization angle is chosen to be a few degrees. Both the beam splitter method and polarization modulation techniques can be used in multi-channel magnetic field measurements.

2.7   Noise Analysis

AM noise in general can be separated into detection system noise and intrinsic spin noise. While many schemes for the detection were demonstrated, usually they are not analyzed in terms of fundamental noise, but rather the experiments are focused on sensitivity demonstrations. Most complete fundamental noise analysis is done in the case of orthogonal beam configurations with the Faraday detection method using a polarizing beam splitter. So this analysis will be discussed in this section in detail.

The sensitivity of probe light polarization measurements is limited by photon shot noise $1/\sqrt{N_{Ph}}$, where N_{Ph} is the number of detected photons. This is because linearly-polarized light can be decomposed into an equal mixture of right and left circularly polarized photons, which numbers fluctuate according to a Poisson distribution. The polarization noise is extremely low, in nrad range, even at moderate laser power of a few mW. At high frequency it can be readily reached, but at low frequency, technical noise often exceeds the photon shot noise.

Apart from this noise, spin-fluctuation noise can also limit the sensitivity. This type of noise occurs due to quantum fluctuations of projections of the spin, which can be estimated from the uncertainty principle. The spin noise scales as $1/\sqrt{N_{Spin}}$, where N_{Spin} is the number of spins in the active volume of the AM. In a typical AM, the fundamental noise is much below 1 fT/Hz$^{1/2}$ and in practical systems, especially at high frequency of operation, the sensitivity is not far off from the fundamental sensitivity.

2.7.1   SERF Sensitivity

High sensitivity of the SERF magnetometer is primarily due to full suppression of SE broadening. The residual magnetic resonance width is determined by spin-destruction rates from interatomic collisions, collisions with the walls, the interaction with the pump and probe beam. In Ref. [19] the fundamental noise of SERF magnetometer has been derived

$$\delta B = \frac{1}{g_S \mu_B P_z \sqrt{nVt}} \sqrt{2\left(R + \Gamma_{pr} + \Gamma_{SD}\right) + \frac{4\left(R + \Gamma_{pr} + \Gamma_{SD}\right)^2}{\Gamma_{pr}(OD)_0}} \qquad (18)$$

where Γ_{SD} is the total collisional spin-destruction rate, Γ_{pr} is the spin-destruction rate due to probe beam, $(OD)_0$ is the optical density at the center of the line, n is the density of alkali-metal spins, V is the active volume of the atomic cell. For typical conditions: $V = 1$ cm^3, density $n = 1.7 \times 10^{13}$ cm^{-3}, $(OD)_0 = 12$, $\Gamma_{SD} = 300\,\mathrm{s}^{-1}$, $R = 710\,\mathrm{s}^{-1}$, and $\Gamma_{pr} = 91\,\mathrm{s}^{-1}$, the Cs AM noise is $\delta B = 0.24\,\mathrm{fT/Hz}^{1/2}$. The second term in this expression can be minimized if $(OD)_0$ is increased, for example, by increasing the density:

$$\delta B = \frac{1}{g_S \mu_B P_z \sqrt{nVt}} \sqrt{2(R + \Gamma_{pr} + \Gamma_{SD})} \tag{19}$$

Then the fundamental noise will be limited by the spin projection noise, which can be in turn optimized by adjusting the pump rate to $R = \Gamma_{SD}/2$ and detuning the probe away from resonance: $\delta B = \frac{3\sqrt{3/2}}{g_S \mu_B} \sqrt{\frac{\Gamma_{SD}}{nVt}}$.

This can be further reduced to the expression

$$\delta B = \frac{3\sqrt{3/2}}{g_S \mu_B} \sqrt{\frac{v\sigma_{SD}}{Vt}} \tag{20}$$

that depends only on a fundamental quantity—the spin-destruction cross section. In case of K, the sensitivity level of aT is possible. By scaling sensitivities with $\sigma_{SD}^{1/2}$ for K, Rb, and Cs, we find that the sensitivity along this sequence changes by an order of magnitude, and even in the case of Cs, it is fairly high. At the moment, the actual question is not much what the fundamental sensitivity is but how closely it can be approached. In each specific case, optimization described above can be accomplished in principle by raising the temperature of the cell. However, there is a limit imposed by properties of glasses and oven design. Cs and Rb require much lower temperature than K, so they can approach the fundamental limit closer. Another important question is the detection sensitivity of the field of a magnetic dipole, which arises in applications of micro-magnetic measurements. Because the field from a dipole falls off cubically with the distance and the field sensitivity scales as square root of the volume, smaller cells actually can win. However, the spin-destruction due to diffusion to the walls can become important to consider and different optimization needs to be carried out. In some detail this question was discussed in [22].

2.7.2 RF AM Sensitivity

Outside the SERF regime, the SE broadening can become very large, with magnetic resonance widths exceeding kHz at typical alkali-metal densities used in SERF magnetometers. To improve sensitivity, it is necessary to use light narrowing, Eq. 9. When the Larmor frequency is relatively low, $\omega_0 \ll v_{HF}$,

$$T_2^{-1} = \frac{R}{4} + \frac{R_{SE}R_{SD}}{5R} \tag{21}$$

(I = 3/2 case). With optimization of the pumping rate, the minimal linewidth is:

$$(1/T_2)_{\min} = (R_{SE}R_{SD}/5)^{1/2} \tag{22}$$

The ratio of this minimal width to the width at very small pump rate, $R_{SE}/8$, gives the light narrowing coefficient, $K = (5\sigma_{SE}/\sigma_{SD})^{1/2}/8$. In the case of potassium, $\sigma_{SE} = 1.8 \times 10^{-14}\,\mathrm{cm}^2$ and $\sigma_{SD} = 1 \times 10^{-18}\,\mathrm{cm}^2$, so the maximum light-narrowing factor is $K_{\max} \approx 37$.

By tuning to resonance and by optimizing the optical pumping, the response of the RF AM to the ac magnetic field can be greatly increased. Because at high frequency the laser technical noise can be removed, for example by using a polarizing beam splitter, the RF AM can be as sensitive as the SERF magnetometer. Fundamental limits of the SERF might be by several orders better, but the RF magnetometer can approach its fundamental limit closer while SERF will be by far dominated by technical noise. The fundamental noise of the RF magnetometer has been investigated in Ref. [6]. After optimization of various parameters, such as the pumping rate and the probe laser intensity, this noise can be expressed in terms of fundamental quantities of atomic vapors, such as SE and SD cross sections:

$$\delta B_{\min} = \frac{2}{\gamma} \sqrt{\frac{\bar{v}[\sigma_{SE}\sigma_{SD}/5]^{1/2}}{V}\left(1 + \frac{1}{4\sqrt{\eta}}\right)} \tag{23}$$

where $\bar{v}$ is the mean thermal velocity of K-K collisions. For a typical photodiode quantum efficiency $\eta = 50\,\%$ and a cell active volume $V = 1\,\mathrm{cm}^3$ cell, the optimized fundamental magnetic field sensitivity is about 0.1 fT/Hz$^{1/2}$.

2.7.3 Intermediate Case Between SERF and RF Magnetometer

In the SERF regime the width is determined by spin-destruction rates, while in the high-frequency RF magnetometer, the width is the function of the SE, SD, and R. In the intermediate regime, the width varies smoothly between minimal in the SERF regime and maximum in the RF magnetometer. This intermediate case can be analyzed using equations for spin-projection noise, photon shot noise, and light-shift noise. However, the width is not a simple analytical function of the SE, SD, and R. Instead numerical simulations of DME are required. Intuitively, we can presume that at optimal conditions the sensitivity will be determined by spin-projection noise and hence scale as

$$\delta B = \frac{1}{g_S\mu_B P_z \sqrt{nVt}} \sqrt{2\left(R + \Gamma_{pr} + \Gamma_{SD} + \Gamma_{extra}\right)} \tag{24}$$

where Γ_{extra} is the contribution arising from spin-exchange collisions, which depends on polarization and magnetic field [26].

2.7.4 Large-Field Scalar AM Sensitivity

If we convert the RF magnetometer to a scalar magnetometer by inducing magnetic-field modulation near the magnetic resonance and by measuring the position of the magnetic resonance, the sensitivity after various optimization steps would be limited by [11]

$$\delta B = \frac{0.77}{\gamma} \sqrt{\frac{v \sigma_{SE}(1 + \eta^{-1/2})}{V}} \tag{25}$$

It is interesting to note that now the sensitivity does not depend on the spin-destruction cross section, as in the case of RF AM. The reason for that is that by applying modulation we reduce the polarization level, which was essentially close to 1 in the case of RF magnetometer, so the light narrowing effect is suppressed. Because SE cross sections are almost the same for K, Rb, and Cs, it follows that the sensitivity of the scalar magnetometer will be quite similar for all three alkali-metal atoms. Moreover, it might not be necessary to heat the cell to high temperatures, as in case of SERF and RF magnetometers. The sensitivity limit of 0.9 fT/Hz$^{1/2}$ is expected for $\sigma_{SE} = 1.8 \times 10^{-14}$ cm^2 and $\eta = 0.8$. It seems that the only way to improve the sensitivity is to increase the volume.

2.7.5 Parallel-Beam AM Sensitivity

The above three cases were considered for the perpendicular pump-probe configuration. The parallel beam configuration has somewhat different result for sensitivity. The spin-projection noise expression would be similar, although the relaxation rate would be larger due to additional contribution of the SE rate arising from relatively large modulation necessary to achieve optimal sensitivity conditions. Alternatively, we can also consider a case when a static field is applied to tilt spins at some angle φ with respect to the pump-probe beam. This essentially would lead to the situation similar to that when the pump and probe beams are perpendicular, except that polarization will be reduced by $\cos(\varphi)$ and the detection signal by additional $\sin(\varphi)$. If we carry out similar optimization as in the previous example, we might conclude that the ultimate limit would come from spin-projection noise and hence the ultimate sensitivity would be not far off from that in the case of the orthogonal configuration.

3   Design and Implementation of an Atomic Magnetometer

3.1   Two-Beam Atomic Magnetometer Scheme

A typical SERF configuration with two orthogonal beams, which was used in first demonstrations of the SERF magnetometer, is shown in Fig. 9. This configuration is the most optimal in terms of sensitivity and is more intuitive for understanding. In case of the high-density RF AM and its scalar derivative, they were implemented only in the two-beam configuration. Furthermore, the two-beam magnetometers are the ones whose fundamental noise was analyzed in the literature.

In the two-beam scheme (Fig. 9), the pump beam is circularly polarized and orients spins along its propagation direction (usually chosen as the Z direction). The Y component of magnetic field rotates the spins from the Z direction into the probe-beam X-direction, and the X-projection of spins (S_x) is detected with a linearly polarized probe beam, which polarization is rotated by atomic vapor (the Faraday effect). Thus, the signal of the AM is proportional to S_x, so the AM signal can be obtained with Eq. (16) in quasi-static approximation. Faraday rotation behaves as dispersive Lorentzian, and the probe beam is detuned from the center of D1 line to maximize the SNR, which is negatively affected by the absorption and spin-destruction by the probe beam, discussed earlier.

The atomic spins are contained in the atomic cell (see below). The cell is heated to increase the density of alkali-metal vapor to the level of 10^{14} cm^{-3}. The alkali-metal atomic spins are polarized and detected with light with high efficiency. Almost 100 % polarization is achieved with the optical pumping method, as we discussed earlier. The pump laser is usually tuned to D1 line (770 nm K, 794 nm Rb, 894 nm Cs) to maximize efficiency and facilitate beam propagation in optically thick vapor. Although many types of lasers can be used and there is no strict requirement on the laser line width, it is found that mode hops produce very large noise and laser stability is important to consider. Distributed feedback (DFB) lasers available for 770 (need cooling to tune from 773 nm) and 794 nm wavelengths are almost ideal due to their low noise and mode-hop-free operation.

The pump and probe (Faraday detection mode) beams require different wavelengths and polarizations, and the best optimization of the sensitivity can be

Fig. 9 A typical SERF magnetometer arrangement. Magnetic field is applied perpendicular to the picture plane
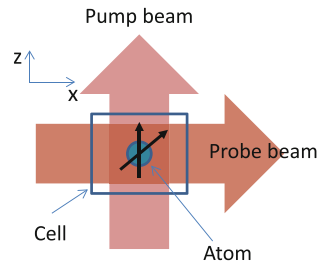
achieved with two separate lasers. In principle, it is still possible to reach high sensitivity with a single laser and a single elliptically polarized beam [24], but this is a compromised solution. The spins in this case are tilted by magnetic field to "imitate" the orthogonal configuration, and the tilt can be made to oscillate to reduce 1/f and other technical noises to compensate for the loss of sensitivity in comparison to the more optimal orthogonal configuration. If absorption instead of Faraday rotation is used to detect spins, then the wavelength in the center of the line and the circular polarization will be optimal for the pump and probe beams [4]. The single-laser parallel-beam schemes are ideal for miniaturization of the design and cost reduction.

3.1.1 Atomic Cell

The atomic vapor cell is the key element of an alkali-metal atomic magnetometer. A typical SERF (RF AM or scalar AM) cell contains a small droplet of K, 1 atm of He to slow-down diffusion, and 30 mtorr of N_2. The diffusion slow-down is important to reduce spin destruction from wall collisions. Helium as a buffer gas provides some advantage because it has the smallest spin-destruction rate with alkali-metal atoms [10]; however, other noble gases and nitrogen can be used as well. In small cells were diffusion spin-destruction start to dominate, nitrogen can be a better choice due to its smaller diffusion coefficient. The nitrogen gas is essential to quench excited states to avoid spin depolarization from spontaneously re-emitted photons. In terms of variation of the cell compositions it is important to optimize the overall spin-destruction rate: the diffusion SD scales inversely with the buffer-gas pressure and inversely quadratically with the size, while the relaxation due to alkali-buffer-gas collisions is proportional to the pressure. From point of view of safety and ease of construction, it is sometimes desirable to use buffer gas at about 1 atm. Pressure as high as 12 atm has been used in experiments where it was necessary to achieve uniform polarization [26]; dealing with such high-pressure cells requires caution since they can explode. Research has also recently focused on realizing a SERF magnetometer using antirelaxation coating rather than buffer gas [35].

Another consideration is the glass material of the cell. Special aluminosilicate glass 1720, which minimizes helium diffusion outside the cell and interaction of alkali-metal atoms with the walls, would be ideal. However, this type of glass is expensive and its availability is limited. Alternatively, Pyrex (borosilicate glass) has been successfully used in SERF magnetometer cells, but at high temperature the diffusion of helium through the glass is significant, and the atomic cell may change its properties over time. To avoid the leakage, neon or nitrogen can replace helium as a buffer gas.

Recently, in SERF magnetometry, trends have been toward miniature cells [4, 36], of less than 1 cm. One issue is that it is more difficult to make a miniature cell with windows of optical quality. In addition, diffusion plays a more important role, and to compensate for its spin-destruction effect, a higher temperature and higher

pressure of buffer gas are needed. Nitrogen, with the largest diffusion slowing, provides an advantage over helium. Having one buffer gas also simplifies the filling procedure.

It is interesting to compare the properties of AMs based on different alkali metals. Potassium of natural abundance, 93.3 % of ^{41}K and 6.7 % of ^{39}K, with both isotopes having the nuclear spin of 3/2, at low field will have atomic spins precessing at one frequency and there will be no negative effect from the mixture. At high field, above the Earth's field magnitude, the resonances will be different and can be resolved. Still, because of small percentage of ^{39}K, only one dominant resonance will be of any consequence. For most applications, the use of pure isotopes won't be necessary. Natural Rb, with 72 % of ^{85}Rb(I = 5/2) and 28 % of ^{87}Rb(I = 3/2) is quite different in this regard. At low frequency, because of difference in slowing down factors, 1/(2I + 1), their precession frequencies will be substantially different and at low density or outside of the SERF regime, the two isotopes will lead to two magnetic resonances or broadening when unresolved. The RF magnetometer will have much smaller light-narrowing effect. In the SERF regime, that is at high densities and low field, the SE rate is much higher than the Larmor frequencies of the two atoms, and the spins will precess with the same frequency and SE relaxation will be suppressed, regardless of the presence of more than one isotope. Thus for high-frequency applications, it is necessary to use isotopically refined Rb, while not in the SERF magnetometer. Cs has only one stable isotope, and does not cause any complication of this kind. A SERF magnetometer typically require densities on the order of 10^{14} cm^{-3} and hence heating to relatively high temperatures (180 °C for K, 160 °C for Rb, and 120 °C for Cs). Various issues related to heating were discussed in the introduction.

3.2 Single Beam Design

As we already mentioned, single-beam or parallel beam designs provide advantages for compact arrangement and low cost. If the Faraday effect is used to detect spins, the magnetometer signal will be proportional to the projection of the spin along the beam. Alternatively, if the absorption is used, the signal will similarly depend on S_z, that is the spin projection along the beam, since absorption is $\exp[-\alpha(1 - P_z)] \approx 1 + \alpha(1 - P_z)$. When the magnetic field is small, S_z variation with the field will be quadratically small and the AM response to a small field will be suppressed. However, when a sufficiently large field is applied that rotates spins away from the Z direction at a significant angle, then the magnetometer becomes linearly sensitive to small fields. The steady-state solution for S_z can be obtained similarly as for S_x but the expression is principally different:

$$S_z = S_0 \frac{1 + (\gamma T_2 B_z)^2}{1 + (\gamma T_2)^2 (B_x^2 + B_y^2 + B_z^2)} \tag{26}$$

Now the signal depends quadratically on all field components, and when they are zeroed, the magnetometer becomes insensitive to small field variations. The maximum response to B_x will be when $B_y = 0$ and $B_z = 0$, but $B_x = B_{x,0}$, then

$$\delta S_z = -S_0 \frac{2(\gamma T_2)^2 B_{x,0} \delta B_x}{\left[1 + (\gamma T_2)^2 B_{x,0}^2\right]^2} \tag{27}$$

This expression can be optimized with respect to the field offset

$$\delta S_z = -S_0 \frac{3\sqrt{3}}{8} \gamma T_2 \delta B_x \approx -0.64 S_0 \gamma T_2 \delta B_x \tag{28}$$

which is about one and a half times smaller than the response of the orthogonal SERF to the B_y field in Eq. 16. It is possible either to measure field when a constant B_x is applied or when it is modulated. Modulation of $B_{x,0}$ provides an advantage of noise reduction by shifting the detection frequency to the region of low-noise. It was found in [24] that by applying large modulation (T_2 also depends on the field, at small fields quadratically, and spin exchange rate), the magnetometer can be optimized and work at modulation of a few kHz. This further reduces the 1/f noise.

3.3 Micro-Fabricated Atomic Magnetometers

It is instructive to investigate how sensitivity depends on the size of the atomic cell. The fundamental noise scales with the combination of nVT_2, so if volume V is reduced, the sensitivity decreases, but it can be partially compensated with the density n, within some limits. The spin-exchange rate and spin destruction rate due to alkali-alkali collisions depend linearly on the density of alkali-metal atoms, while other rates are density independent, and thus raising the density improves sensitivity until alkali-alkali collisions start to dominate the spin-destruction rate. With the size reduction, the spin-destruction due to diffusion to the walls, which scales inversely with the area, become more important. It can be reduced by using N_2 as a buffer gas, which has a smaller diffusion coefficient than helium, traditionally used in SERF due to its smallest spin-destruction rate with alkalis. Raising buffer-gas pressure is another measure for optimization. On the other hand, small cells require much less power and the whole package can be micro-fabricated to reduce the cost. The analysis of the size-dependent sensitivity is provided in [36].

3.4 Multi-channel Magnetometers

In many applications, such as source localization in MEG and MCG, simultaneous detection of a magnetic field in multiple points is required. Commercial SQUID-based MEG systems have hundreds of channels; the two main problems with these systems are cryogenic operation and high cost. If SQUIDs are replaced with atomic magnetometers, cryogenic requirement will be eliminated, but the price of building hundreds of atomic magnetometers can still be very high. The price can be reduced if various elements of atomic magnetometers are shared. For example, instead of having a separate laser for each magnetometer, laser power can be amplified and distributed among multiple magnetometers, saving the cost for laser electronics and optics, such as optical isolators. Additional savings on optics and atomic cells can be achieved by using a large atomic cell that is imaged with a broad beam [2]. Such sharing is possible because buffer gas restricts the diffusion of atoms to less than cm distances ($\sqrt{D_0 t}$, where D_0 is the diffusion coefficient and t diffusion time), so that multiple regions of a 10-cm cell can independently measure field at as many as hundred points. The only drawback of such a multi-channel system is geometry: in MEG systems for full coverage the sensors have to be inserted in a helmet configuration, which is impossible with one large cell. Still, by positioning such multi-channel large-cell magnetometers at several head locations, more or less complete coverage can be achieved. Demonstration of multi-channel MEG with a large cell was given in Ref. [2]. On the other hand, for MCG applications, a flat geometry is almost ideal, and only one multi-channel AM would be needed.

Applications in MRI also can benefit from multi-channel operation to save the cost. At low frequency, the multi-channel AM can be directly used, but at high frequency a difficult problem exists that NMR and AM fields have to be 400-time different. One solution that would work for anatomical MRI is addition of flux transformers. Multiple flux transformers, which are inductively decoupled, can be used to realize multi-channel parallel imaging [37].

3.5 Design Issues

3.5.1 Lasers

Lasers have been essential to the success of high-sensitivity magnetometers. It is important to have high-quality lasers for both pumping and probing, although in some cases, requirements can be relaxed. The effects of laser instabilities and noise on the AM sensitivity are different in cases of pump and probe lasers. Fluctuations in pump intensity and wavelength can lead to light-shift noise in the pump direction, which is equivalent to fluctuating magnetic field along this direction. This technical noise can easily become dominant source of noise; however, it is possible

suppress it in the SERF magnetometer by zeroing the field along the probe direction if the pump and probe beams are orthogonal. Another way to suppress this noise is to choose a laser wavelength that will minimize light shift fluctuations. As we previously discussed, light shift is proportional to the light intensity and depends on wavelength as a dispersion Lorentzian, crossing zero at the center of the absorption line. Minimum fluctuations in the light shift due to intensity variation will occur when the laser is tuned to the line center, while minimum light shift fluctuations due to wavelength instability will be when the laser is detuned from the center by one line width. Depending on the dominant nature of fluctuations, the pump laser can be tuned accordingly to minimize the light shift noise. When AM is operating in the scalar magnetometer mode, i.e. measuring the z component of the field, the light shift cannot be reduced by zeroing the B_x field (along the probe beam), thus it is highly desirable to use a high-quality pump laser.

The requirement for a probe laser is even more demanding since the probe noise contributes to the magnetometer noise directly. If the probe beam is detuned away from the D1 or D2 line by several linewidths, the effect of wavelength fluctuations is suppressed, and intensity fluctuations can become more important. (Although we note that the analysis of wavelength fluctuation effects was not conducted in the literature.) For this reason, a polarizing beam splitter is used to reduce the effect of intensity fluctuations. When carefully balanced, the polarimeter based on the PBS can suppress the intensity fluctuation 30 times or even more, ideally to the level of photon shot noise. Some asymmetry in the detection channels for the two beams leads to the reduction in noise suppression. So it is important to have high quality lasers to avoid additional technical noise.

It has been found that DFB lasers have very good noise performance. Their noise level with PBS starting with relatively low frequency is close to photon-shot noise limit. Lasers with gratings that are not very rigidly attached generate more noise, and mode hops occur frequently that result in very large noise, requiring adjusting the laser current and temperature. Long-term measurements with such lasers are often problematic. Multi-mode lasers are not generally suitable for high-sensitivity low-frequency magnetometers. However, at high frequency, noise usually approaches photon-shot noise, even in inexpensive lasers. Thus RF magnetometers have less stringent requirements on the lasers. The scalar magnetometer, on the other hand, although its signal is detected at high frequency (in Earth's field, at about 350 kHz), is sensitive to pump beam light shift at low frequency. Thus requirement on the pump laser might be more stringent than for the probe laser.

3.5.2 Fiber-Coupling

Fiber-coupling has been used to reduce price and add flexibility in measurements. It has been found that the light beam generated by a DFB laser after passing through a fiber (for example, a PM fiber) does not have excessive noise. Thus a head of a magnetometer, which contains the cell, can be spatially separated from other supporting equipment as much as 5 m. Both single-beam [3, 4, 24] and two-beam [16]

fiber-coupled designs have been developed. Also DFB lasers have been used that were fiber-coupled removing the need for extra optical components required to inject the light into a single mode fiber [16]. However, feedback from the fiber attached to the laser can lead to instabilities, and substantial increase in noise in the schemes where PBS is not used. Thus it is still preferable to have an external coupler with an optical isolator, despite extra cost and complexity of design.

3.5.3   Commercial Designs

Fiber-coupled designs have been commercialized by Twinleaf and QuSpin companies. The sensitivity on the order of 10 fT/Hz$^{1/2}$ has been demonstrated. The magnetometers are in the process of further development. One direction is to make the magnetometer user-friendly, so the operator does not need to tune fields, lasers, etc. manually. Once the magnetometers become widely available they would strongly compete with SQUIDs in many demanding applications such as MEG.

3.6   Sensitivity Demonstrations

Sensitivity demonstrations are the most important aspect of the research on atomic magnetometers. The first significant milestone was the demonstrations of superior sensitivity by SERF magnetometer [1]. Then various designs of SERF, RF, and scalar magnetometers have been explored with sensitivity demonstrations and analysis. In particular, an RF magnetometer has demonstrated sensitivity of 0.2 fT/Hz$^{1/2}$ adopted for NQR detection [28]. Many groups now were able to achieve fT sensitivity with various designs, which were aimed at specific goals, such as MEG, cost reduction, simplification of design, or micro-fabrication. Fiber-coupled designs are approaching the sensitivity of the original optical table AMs, and there is a potential for further improvement [4, 16]. The highest sensitivity to date in SERF regime was demonstrated by Princeton using vacuum-enclosed optical design [13]. Scalar magnetometers, although less sensitive than SERF magnetometers, have been of great interest to geophysical and military applications, when the magnetometer needs to operate at ambient field. Substantial advantage of scalar magnetometers is their invariance with respect to field rotation, so vibration and orientation instabilities do not lead to large noise. Unfortunately, due to multiple hyperfine structure Zeeman levels, with splitting non-linear in the Earth's field, the magnetometer has its frequency slightly sensitive to field rotation. The demonstration of high sensitivity of a scalar magnetometer based on RF AM was recently given [11]. The analysis showed that this is close to the fundamental limit. However, further improvements were found, using for example multi-pass approach [38].

4 Applications

4.1 Comparison with SQUID

SERF AMs and SQUIDs are the most sensitive magnetometers at low frequencies. Although it is also possible to construct a large coil that can have fT sensitivity, many applications introduce restrictions on weight and size, and at very low frequency, coils become problematic. SQUID technology has been around for decades and matured enough to be readily available from a company; however, SERF, scalar, and especially RF magnetometers are just at the initial stage of technology readiness. From point of view of sensitivity, SERF magnetometers should be able to replace SQUIDs in most applications, but both SERF and SQUIDs have application limits stemming from their physical principles. Non-cryogenic operation of SERF is the main strength of this technology. Supply of expensive liquid helium is limited and requirement for cryogenic infrastructure is restrictive. Apart from this, SQUID systems also require maintenance. Also important is that thermal electrically conductive shields, needed for improving the efficiency of cryogenic cooling, produce excessive noise, degrading the performance of SQUID systems and making practical SERF magnetometers more sensitive.

Unlike SQUIDs, SERF magnetometers are not used with superconducting flux transformers (SFT), which configured as gradiometers in SQUID systems, reject common-mode magnetic noise by several orders of magnitude enabling operation in poorly shielded environments. Alternatively configured as gradiometers from several magnetometers [4] or channels in large-cell multi-channel systems [2], SERF magnetometers do not provide as large common-mode noise suppression. This is due to instability of the magnetometer signals, which depend on many parameters. In the presence of gradients, SERF magnetic resonances are broadened and sensitivity is reduced, while SQUID gradiometers with feedbacks can operate in a relatively large dc field and are insensitive to dc gradients.

In contrast to SQUIDs, the SERF magnetometer also needs to be zeroed to operate with maximum sensitivity. In the Earth's field environment, this can be done with a three-axis Helmholtz coil system, but gradients and magnetic field fluctuations negatively affect the sensitivity [39]. When SERF or RF magnetometers are used for NMR or MRI detection, the AMs need to be decoupled from NMR and MRI fields [5, 40]. SQUIDs decoupled with SFT do not compromise the sensitivity, but using AMs is problematic. Several methods have been developed for this, but each has some issues [5, 40–42].

SERF and SQUID have also different bandwidths (BW). In case of SERF, there is inverse relation between BW and the sensitivity, and SERF magnetometers with fT sensitivity do not have BW exceeding much 100 Hz. SQUIDs, on the other hand, can have response in a very large frequency range. The dc SQUID BW is only restricted by a feedback system that has finite BW. In systems used for ULF-MRI detection, BW has been on the order of several kHz, with sensitivity still in fT range. But the large BW of SQUIDs is their liability, making them sensitive to

noise in the frequency range from dc to microwaves. High-frequency noise can be effectively reduced with Mylar® foil, but this foil produces noise on the order of a few fT, reducing SQUID sensitivity. SERF does not need protection against high-frequency noise. Low frequency noise is important to remove.

In terms of operation temperature, the SERF magnetometer cell is heated above 100 °C while SQUIDs are kept in LHe Dewar (high-Tc variety is less sensitive). In both cases, effective thermal insulation is required to reduce the stand-off distance to the measured object.

Despite various problematic issues with SERF and other atomic magnetometers, the absence of cryogens is the principal benefit that would lead to replacement of SQUIDs in a wide range of applications.

4.2 Biomedical Applications of High-Density AMs

Research on atomic magnetometers is strongly motivated by many current and potential future applications. Among such applications, MEG is probably the most invaluable because no other device than the atomic magnetometer can rival low-Tc SQUIDs in sensitivity at low frequency, in the range of interest to MEG.

4.2.1 MEG Applications of SERF Magnetometers

MEG history starts with the first magnetic recordings of brain activity with a Faraday coil [43], which served as the proof of principle of existence of the brain magnetic field. Shortly after the first demonstration, the sensitivity was dramatically improved with a SQUID magnetometer [44], and tater on, multi-channel systems have been introduced for MEG source localization. After further development, the multi-channel systems became the basis for MEG research and clinical applications. However, the cost of MEG systems that included the price of liquid helium, maintenance, magnetically shielded rooms, and other expenses have been very high, resulting in modest propagation of the MEG method into the clinical practice and research. Some work has been directed toward cost reduction, such as construction of SQUID gradiometers that do not require expensive multi-layer shielded rooms for MEG measurements, but all practical MEG systems have been based on SQUIDs requiring liquid helium supply.

However, MEG systems can be also based on atomic magnetometers to eliminate the need for cryogens. In 2006, the first demonstration was done [2] and it was reasoned that a commercial multi-channel system can be built at a fraction of cost of a multi-channel SQUID system. As we have already discussed it, there are several strategies for cost reduction, including an inexpensive multi-channel operation, possible with a large atomic cell. In addition, because AM do not require a large Dewar, a low cost shield can be designed for subjects in a reclining position consisting of mu-metal cylinders [2]. Unfortunately, the demonstrated design was

not yet suitable for a full-head MEG system that is needed for medical applications. However, the work AM-MEG has been continued. Instead of building SERF magnetometers with large cells, several groups focused on AM-MEG demonstrations with separate AM sensors with the goal in reduction cost per channel. In particular, fiber-coupled sensors were developed that could reach sensitivity of a few fT and these sensors were applied to detect MEG signals [3, 4, 45]. Currently the cost of building hundreds of AM channels is relatively high, but it is hoped that with mass-production development, this cost can be significantly reduced.

4.2.2   Other Applications of SERF and High-Density Magnetometers

Magnetocardiography

Magnetocardiography (MCG) in general requires lower sensitivity than MEG and is another promising direction for applications of SERF and other atomic magnetometers. Since heart anomalies are among leading causes of death, their diagnosis is extremely important, and AM MCG could become an invaluable tool for saving millions of lives. Multi-channel MCG provides information on electrical activity in the heart non-invasively, and hence this modality can be crucial for revealing heart anomalies and the analysis of their localization. With high sensitivity and multi-channel detection capability of SERF, more sensitive diagnostics of heart anomalies can be developed. Already, FDA approval has been obtained for diagnostics of women heart conditions with MEG, and study was conducted that showed that the MCG diagnostics is much more reliable than other methods. Although the clinical trials were conducted with SQUIDs, it is clear that they can be replaced with AMs to relieve the requirement for cryogens. Potentially lower cost of construction of multi-channel system and of maintenance will facilitate wide spread of the AM-based MCG method and make it competitive with inexpensive conventional technology such as ECG. Compared to MEG, MCG application will require only one or two multi-channel magnetometers with large cells: one positioned on the chest area and the other on the back. SQUIDs are held in a Dewar and in general are only positioned above the patient, but better diagnostics can be performed with more complete coverage.

Detection of Magnetic Nano-Particles

Another class of medical applications is based on nano-particle detection. For example, it has been found that magnetic nanoparticles of specific size attached to cancerous cells have a specific magnetization variation after alignment with a strong field. Again SQUIDs were used to pioneer this diagnostic method, but future is quite promising for AMs as well. The main problem is the need to conduct measurements in unshielded environment, but SERF magnetometers are not ideal in this

situation. It would be necessary to set up a gradiometric operation that would cancel fairly large magnetic field noise in ambient clinical environment.

NMR and MRI Applications

High sensitivity of atomic magnetometers can be important for applications in unconventional low- and ultra-low field (ULF) NMR and MRI. One motivation for exploring ULF MRI is that it is not based on bulky and expensive superconducting or permanent magnets and some applications complementary to conventional MRI can be developed. One example of such application is combined MEG and MRI [46] that can reduce the co-registration error. Another class of novel applications can exploit unique properties of ULF MRI such as low cost and portability. In long run, ULF MRI scanners can lead to increased availability of MRI diagnostics around the world. However, obtaining clinically useful images at ULF is fraught with challenges. First, because NMR/MRI is detected with a pick-up coil, which output is the time derivative of the magnetic flux (Faraday's law), SNR is severely compromised at low frequency. Second, the polarization of nuclear spins is very weak in ultra-low field further reducing SNR. To make things worse for a developing technology, conventional MRI has set very high standards of image quality: with high resolution, high SNR, and fast imaging.

To some extent, the compensation for a weak signal in the ULF regime can be made with the pulsed-prepolarization method, in which a much larger field is applied to polarize nuclear spins (e.g. [47]). During the detection stage this field is removed, so it does not affect the ULF or LF signal read-out. However even with prepolarization enhancement, the SNR and resolution are still poor. Some progress has been made with replacement of coils with SQUIDs to improve the sensitivity at low frequency and to realize multi-channel parallel MRI acceleration [46]. This of course brought the problem of cryogenic operation. To amend this, AMs have been proposed to replace SQUIDs.

The most potentially useful AM magnetometer for MRI applications is the high-density RF atomic magnetometer [5]. The RF magnetometer has several useful features: (i) very high sensitivity with fundamental limit about 0.1 fT/Hz$^{1/2}$ for 1 cm^3 cell [6] and demonstrated sensitivity in a large cell 0.2 fT/Hz$^{1/2}$ [28]; (ii) sufficient bandwidth, reaching a kHz range, much larger than that of other AMs; (iii) operation at high frequency where ambient noise is lower; (iv) low cost and finally multi-channel operation [37]. The first demonstration of MRI with AM in the configuration that is suitable for anatomical imaging was done in 2009 [40] and actual anatomical imaging with RF AM was achieved in 2013 [48]. The latest achievements are the demonstration with AM of MRI of the human brain [49] and multi-channel operation [37].

With regard to MRI applications, it is important to remember that while the sensitivity of SQUIDs and AMs is about the same, the AM is highly sensitive to static fields and gradients, while SQUIDs are to a large extent immune to them. The field affects the AM frequency of maximum response—in fact it is applied to tune

the AM to a specific frequency, while the gradients broaden atomic magnetic resonances and reduce sensitivity.

In direct MRI detection, the MRI field and gradients need to be removed at the AM sensor location. The difference in gyromagnetic ratios between protons and K (Rb-87) spins is about 400, so the gradient applied in MRI will broaden the AM BW 400 times, well beyond that required for optimal operation. For these reasons, AMs in general are more problematic for MRI applications than SQUIDs, but solutions for these problems exist.

One strategy for detection MRI signal with AM is to do it remotely [42], with the liquid sample arranged to flow from a pre-polarization region and an encoding region to a detection region. The prepolarization can be done with a strong non-uniform permanent magnet, while the detection region can be isolated from environment noise and external field with a ferromagnetic shield. The main disadvantage of remote detection is that the sample needs to be moved, which is difficult in the case of anatomical imaging. As the result, anatomical imaging has not been demonstrated with this approach.

The second strategy is detection at ultra-low frequency ($\sim$ kHz) with the sample placed in a solenoid to separate the NMR and AM fields [41]. Because of ultra-low field, the field separation with a not-ideal solenoid does not lead to artifacts. With additional work on perfecting the solenoid, this approach can be in principle extended to frequencies on the order of 100 kHz [5], but there are other factors that would limit applications: the solenoid has to be long preventing easy access for anatomical imaging; more importantly, imaging gradients are very large and will broaden magnetometer resonance and decrease its sensitivity.

The most currently feasible approach for anatomical imaging with an AM is the detection mediated with a flux transformer (FT) (Fig. 10) [40]. FTs are widely used with SQUID magnetometers, where they are cryogenic and superconducting. The FT consists of two coils, an input coil that generates voltage from the MRI signal, and an output coil, electrically connected to the input coil, that generates magnetic field. Basically FT transfers magnetic field from the MRI region to the detection region. The input coil can be configured as a gradiometer to reduce noise. The output coil is placed near a magnetometer, SQUID or AM. AMs can be in principle used with a cryogenic FT, but the overall advantage of non-cryogenic operation would be lost. We have recently demonstrated MRI using a room-temperature (RT) FT. The room temperature FT brings flexibility in the positioning and simplicity in operation. RT FT removes the dc and attenuates low-frequency components of the field and gradients, solving the problem of decoupling AM and MRI field systems. However, the RT operation comes at the price of additional Johnson noise. Because with frequency the Johnson noise as well as the noise of surrounding metallic parts decreases, the increase in frequency can be a very efficient method for noise reduction.

Additional benefit of the FT-AM detection scheme is the increase in the bandwidth (BW) when the FT is detuned from the AM magnetic resonance (Fig. 11). Larger BWs are needed for high-resolution imaging and for fast multi-pulse imaging methods. This can be illustrated with an example. For a 100-ms acquisition

Fig. 10 Atomic
magnetometer and flux
transformer setup (*top*) and its
diagram (*bottom*). Adopted
from [37]
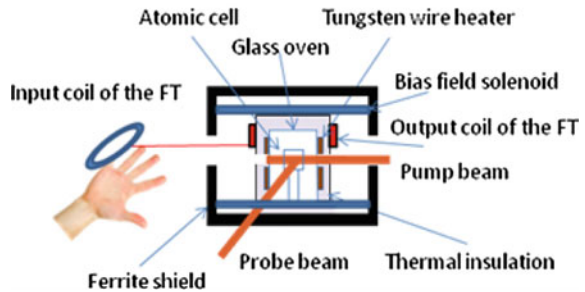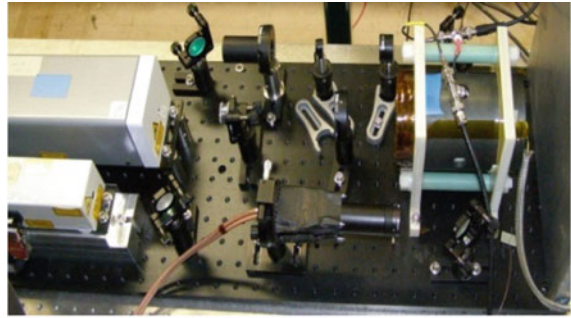
Fig. 11 Illustration of BW
enhancement of AM+FT
detection method, without
loss in sensitivity [48]
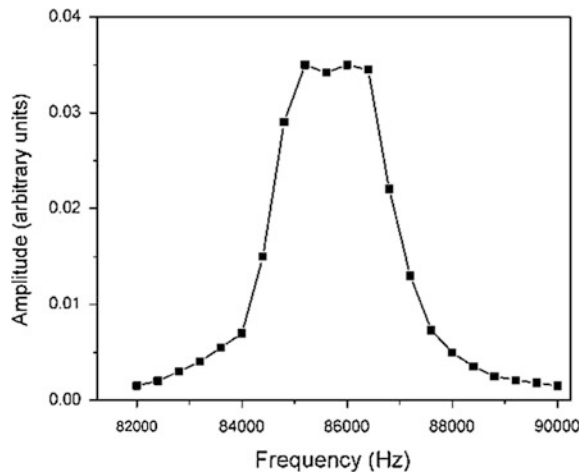
time, typically used in ULF MRI, the required BW per pixel is 10 Hz. Fifty-pixel
image in the read-out direction translates into 500-Hz BW, and if a
Car-Purcell-Meiboom-Gill (CMPG) sequence with 5 pulses per excitation is
employed, the BW will be needed as large as 2.5 kHz. A typical RF AM has BW
on the order of 200 Hz, so from this estimate it cannot obviously be used for fast
sequences, but the FT-AM detector will be suitable.

Other Potential Applications Based on High Sensitivity

There are many other potential applications of AMs which can be developed where high sensitivity is required. For example, AMs can be used in submarine detection, geology, archeology, military applications. Currently, high-sensitivity AMs are becoming commercially available, and this will certainly increase the range their applications.

Fundamental experiments

Some of the most fascinating applications are in the academic world, for example in tests of fundamental symmetries. Here cryogenic operation of SQUIDs is not a big problem, but still AMs have some unique properties that they themselves become the objects of research. An example of such an application is the measurement of electric dipole moments (EDM) of atoms. There are several schemes for EDM experiments. The basic idea is to apply a strong electric field and to measure with high sensitivity a weak magnetic field arising due to EDM. Because the hypothetical atomic EDMs are extremely small, it is necessary to use sensors of highest possible sensitivity. Some schemes are based on unique properties of atomic spins and such experiments cannot be done with arbitrary magnetic sensors. Others do not necessarily need atomic magnetometers, and low-Tc SQUIDs are used as more conventional commercially available sensors. Early EDM experiments and theoretical calculations are reviewed in [50].

Atomic magnetometers, or rather co-magnetometers, were also used in fundamental CPT violation experiments and recently a new limit was set [51, 52].

Basic research in atomic magnetometers

While atomic magnetometers are great for the multitude of their applications, on the basic science side, also there are many activities. Setting new limits or demonstration of new principles and configurations have been one focus of such activities.

5 Conclusions

We have discussed ultra-sensitive atomic magnetometers based on high-density alkali-metal vapors. This chapter covers the principles of the operation of ultra-sensitive magnetometers and their applications. Among applications MEG and ULF MRI have been considered in some detail. Because low-Tc SQIUDs have been known as the most sensitive magnetometers for a long time and are still considered such by many researchers, the important conclusion from this chapter should be that atomic magnetometers can provide similar sensitivity and can be used instead of SQUIDs in many applications.

References

1. I.K. Kominis, T.W. Kornack, J.C. Allred, M.V. Romalis, A subfemtotesla multichannel atomic magnetometer. Nature **422**, 596 (2003)
2. H. Xia, A. Ben-Amar Baranga, D. Hoffman, M.V. Romalis, Magnetoencephalography with an atomic magnetometer. Appl. Phys. Lett. **89**, 211104 (2006)
3. K. Johnson, P.D.D. Schwindt, M. Weisend, Magnetoencephalography with a two-color pump-probe, fiber-coupled atomic magnetometer. Appl. Phys. Lett. **97**, 243703 (2010)
4. V. Shah, R.T. Wakai, A compact, high performance atomic magnetometer for biomedical applications. Phys. Med. Biol. **58**, 8153–8161 (2013)
5. I.M. Savukov, S.J. Seltzer, M.V. Romalis, Detection of NMR signals with a radio-frequency atomic magnetometer. JMR **185**, 214 (2007)
6. I.M. Savukov, S.J. Seltzer, M.V. Romalis, K.L. Sauer, Tunable atomic magnetometer for detection of radio-frequency magnetic fields. Phys. Rev. Lett. **95**, 063004 (2005)
7. E. Harel, L. Schröder, S. Xu, Annu. Rev. Anal. Chem. **1**, 133 (2008)
8. G. Bison, R. Wynands, A. Weis, Opt. Express **11**, 904–909 (2003)
9. B. Patton, A.W. Brown, R. Slocum, E.J. Smith, in *Ch. 15, Space Magnetometry*, ed by D. Budker, D.F.J. Kimball. Optical Magnetometry (Cambridge University Press, Cambridge, 2013), pp. 285–302
10. J. Allred, R. Lyman, T. Kornack, M. Romalis, A high-sensitivity atomic magnetometer unaffected by spin-exchange relaxation. Phys. Rev. Lett. **89**, 130801 (2002)
11. S.J. Smullin, I.M. Savukov, G. Vasilakis, R.K. Ghosh, M.V. Romalis, A low-noise high-density alkali-metal scalar magnetometer. Phys. Rev. A **80**, 033420 (2009)
12. W. Happer, H. Tang, Phys. Rev. Lett. **31**, 273 (1973)
13. H.B. Dang, A.C. Maloof, M.V. Romalis, Ultrahigh sensitivity magnetic field and magnetization measurements with an atomic magnetometer. Appl. Phys. Lett. **97**, 151110 (2010)
14. P.D.D. Schwindt, S. Knappe, V. Shah, L. Hollberg, J. Kitching, Chip-scale atomic magnetometer. Appl. Phys. Lett. **85**, 6409 (2004)
15. T.W. Kornack, S.J. Smullin, S.K. Lee, M.V. Romalis, Appl. Phys. Lett. **90**, 223501 (2007)
16. I. Savukov, T. Karaulanov, M. Boshier, Ultra-sensitive high-density Rb-87 radio-frequency magnetometer. Appl. Phys. Lett. **104**, 023504 (2014)
17. T.G. Walker, W. Happer, Spin-exchange optical pumping of noble-gas nuclei. Rev. Mod. Phys. **69**, 629–642 (1997)
18. S. Kadlecek, L.W. Anderson, T. Walker, Measurement of potassium-potassium spin relaxation cross sections. Nucl. Instrum. Meth. Phys. Res. A **402**, 208–211 (1998)
19. M.P. Ledbetter, I.M. Savukov, V.M. Acosta, D. Budker, M.V. Romalis, Spin-exchange-relaxation-free magnetometry with Cs vapor. Phys. Rev. A **77**, 033408 (2008)
20. M.P. Ledbetter, I.M. Savukov, D. Budker, V. Shah, S. Knappe, J. Kitching, D.J. Michalak, S. Xu, A. Pines, Zero-field remote detection of NMR with a microfabricated atomic magnetometer. Proc. Natl. Acad. Sci. USA **105**, 2286 (2008)
21. S. Knappe, P. D. D. Schwindt, V. Gerginov, V. Shah, L. Liew, J. Moreland, H. G. Robinson, L. Hollberg, J. Kitching, Microfabricated atomic clocks and magnetometers. J. Opt. A Pure Appl. Opt. **8**, S318–S322 (2006)
22. V. Shah, S. Knappe, P.D.D. Schwindt, J. Kitching, Subpicotesla atomic magnetometry with a microfabricated vapour cell. Nat. Photonics **1**(11), 649–652 (2007)
23. W.C. Griffith, S. Knappe, J. Kitching, Opt. Express **18**, 27167 (2010)
24. V. Shah, M.V. Romalis, Spin-exchange relaxation-free magnetometry using elliptically polarized light. Phys. Rev. A **80**, 013416 (2009)
25. Twinleaf, [Online]. Available: http://www.twinleaf.com/
26. I.M. Savukov, M.V. Romalis, Effects of spin-exchange collisions in a high-density alkali-metal vapor in low magnetic fields. Phys. Rev. A **71**(2), 023405 (2005)

27. S. Appelt, A. Ben-Amar Baranga, A.R. Young,. H.W. Young, Light narrowing of rubidium magnetic-resonance lines in high-pressure optical-pumping cells. Phys. Rev. A **59**, 2078–2084 (1999)

28. S.-K. Lee, K. Sauer, S.J. Seltzer, O. Alem, M.V. Romalis, Subfemtotesla radio-frequency atomic magnetometer for detection of nuclear quadrupole resonance. Appl. Phys. Lett. **89**(21), 214106 (2006)

29. G. Breit, I.I. Rabi, Measurement of nuclear spin. Phys. Rev. **38**(11), 2082 (1931)

30. W. Happer, W.A. van Wijngaarden, An optical pumping primer. Hyperfine Interact. **38**(1), 435–470 (1987)

31. W. Happer, A.C. Tam, Effect of rapid spin exchange on the magneticresonance spectrum of alkali vapors. Phys. Rev. A **16**(5), 1877–1891 (1977)

32. W. Happer, Optical pumping. Rev. Mod. Phys. **44**, 169–250 (1972)

33. A. Appelt, B.-A. Baranga, C.J. Erickson, M.V. Romalis, A.R. Young, W. Happer, Theory of spin-exchange optical pumping of 3He and 129Xe. Phys. Rev. A **1412–1439**(2), 58 (1998)

34. I. Savukov, Gradient-echo 3D imaging of Rb polarization in fiber-coupled atomic magnetometer. JMR **256**, 9–13 (2015)

35. S.J. Seltzer, M.V. Romalis, J. Appl. Phys. **106**, 114905 (2009)

36. V. Shah, S. Knappe, P.D.D. Schwindt, J. Kitching, Subpicotesla atomic magnetometry with a microfabricated vapour cell. Nat. Photonics **1**, 649–652 (2007)

37. I. Savukov, T. Karaulanov, Multi-flux-transformer MRI detection with an atomic magnetometer. JMR **249**, 49–52 (2014)

38. D. Sheng, S. Li, N. Dural, M.V. Romalis, Subfemtotesla scalar atomic magnetometry using multipass cells. Phys. Rev. Lett. **110**, 160802 (2013)

39. S.J. Seltzer, M.V. Romalis, Unshielded three-axis vector operation of a spin-exchange-relaxation-free atomic magnetometer. Appl. Phys. Lett. **85**(20), 4804 (2004)

40. I.M. Savukov, V.S. Zotev, P.L. Volegov, M.A. Espy, A.N. Matlashov, J.J. Gomez, R.H. J. Kraus, MRI with an atomic magnetometer suitable for practical imaging applications. JMR **199**, 188–191 (2009)

41. I.M. Savukov, M.V. Romalis, NMR detection with an atomic magnetometer. Phys. Rev. Lett. **94**, 123001 (2005)

42. S. Xu, S. Rochester, V.V. Yashchuk, M. Donaldson, D. Budker, Rev. Sci. Instrum. **77**, 083106 (2006)

43. D. Cohen, Magnetoecephalography: evidence of magnetic field produced by alpha- rhythm current. Science **161**, 784–786 (1968)

44. D. Cohen, Magnetoencephalography: detection of the brain's electrical activity with a superconducting magnetometer. Science **175**, 664–666 (1972)

45. T.H. Sander, J. Preusser, R. Mhaskar, J. Kitching, L. Trahms, S. Knappe, Magnetoencephalography with a chip-scale atomic magnetometer. Biomed. Opt. Express **3**, 981 (2012)

46. V.S. Zotev, A.N. Matlashov, P.L. Volegov, I.M. Savukov, M.A. Espy, J.C. Mosher, J. J. Gomez, R.H.J. Kraus, Microtesla MRI of the human brain combined with MEG. JMR **194**, 115–120 (2008)

47. A. Macovski, S. Conolly, Novel approaches to low-cost MRI. Magn. Reson. Med. **30**(2), 221–230 (2005)

48. I. Savukov, T. Karaulanov, Anatomical MRI with an atomic magnetometer. JMR **231**, 39–45 (2013)

49. I. Savukov, T. Karaulanov, Magnetic-resonance imaging of the human brain with an atomic magnetometer. Appl. Phys. Lett. **103**, 043703 (2013)

50. I.B. Khriplovich, L.S.K. Khriplovich, *CP Violation Without Strangeness: Electric Dipole Moments of Particles, Atoms, and Molecules* (Springer, Berlin, 1997)

51. J.M. Brown, S.J. Smullin, T.W. Kornack, M.V. Romalis, New limit on lorentz-and CPT-violating neutron spin interactions. Phys. Rev. Lett. **105**, 151604 (2010)

52. M. Smiciklas, J.M. Brown, L.W. Cheuk, S.J. Smullin, M.V. Romalis, New test of local lorentz invariance using a 21Ne–Rb–K comagnetometer. Phys. Rev. Lett. **107**, 171604 (2011)